Anisotropic exchange and spin dynamics in the type-I (-IA) antiferromagnets CeAs, CeSb, and USb: A neutron study

B. Hälg and A. Furrer
Eidgenössische Technische Hochschule Zürich, Labor für Neutronenstreuung, CH-5303 Würenlingen, Switzerland
(Received 24 April 1986)

The anomalous anisotropic magnetic interactions and the spin dynamics of the fcc type-I or -IA antiferromagnetic cerium and uranium monopnictides CeAs, CeSb, and USb have been studied by inelastic and diffuse critical neutron scattering experiments. The diffuse scattering above the antiferromagnetic ordering temperature largely corresponds to longitudinal spin fluctuations which are highly anisotropic. In the ordered state the dispersion curves of the spin-wave excitations strongly depend on the actually realized spin structure. For the antiferromagnets the spin waves split into transverse modes with different polarizations due to the exchange anisotropy. In CeAs one of these modes exhibits nearly zero energy gap and quadratic dispersion which has not previously been observed in antiferromagnets. The wave-vector-dependent susceptibility tensor has been calculated within the random-phase-approximation (RPA) by taking account of crystal-field, anisotropic bilinear exchange, and isotropic quadrupolar interactions. General expressions including all levels of the ground-state multiplet are derived for single-**q** and triple-**q** type-I as well as for type-IA antiferromagnets, and detailed formulas of the magnetic excitation spectrum are given for the particularly interesting case of effective two-level systems which are often realized in f-electron magnets. The RPA formalism consistently describes the transverse magnetic excitations for $T < T_N$ as well as the longitudinal spin fluctuations for $T > T_N$ for all compounds under study. For CeAs and CeSb the bilinear exchange interactions turn out to be similar, and evidence for important effects of higher-order magnetic interactions is found. The latter are shown to be the driving mechanism for the realization of the various magnetic phases in CeSb. For CeAs the magnetic excitation spectrum unambiguously demonstrates that a collinear single-**q** type-I spin structure is realized, whereas for USb a noncollinear triple-**q** type-I spin structure emerges from the observed magnetic excitations.

I. INTRODUCTION

All the cerium and uranium monopnictides (CeX and UX with X=N,P,As,Sb,Bi) crystallize in the face-centered-cubic (fcc) NaCl structure. At low temperature they exhibit unusual magnetic properties, the most striking phenomenon being the existence of strongly anisotropic magnetic interactions. For the majority of these compounds antiferromagnetic type-I (AF-I) ordering is observed, in which ferromagnetic (001) planes are stacked in a $+-+-$ sequence.[1] Exceptions are CeN, which does not order magnetically, and CeSb, which exhibits a large number of commensurate magnetic phases corresponding to a characteristic stacking of nonmagnetic and ferromagnetic (001) planes.[2,3] At $T \sim T_N/2$ CeBi and UAs undergo a first-order transition to the antiferromagnetic type-IA (AF-IA) structure corresponding to a $++--$ stacking; this is also the low-temperature phase of CeSb.[3] In CeSb (Refs. 4 and 5) and CeBi (Ref. 5) a significant tetragonal distortion was observed at T_N, whereas the other compounds show no detectable distortion in conjunction with magnetic ordering. Some magnetic properties of CeX and UX are listed in Table I.

The magnetic properties of CeX and UX originate in the $4f$ or $5f$ electrons of Ce^{3+} and U^{3+}, respectively. Whereas for CeX the electrons are localized, the UX systems show an increasing delocalization of the $5f$ electrons towards the lighter pnictides. The most central problem associated with the CeX and UX compounds is the anomalous anisotropy of the magnetic interactions in these systems. One mechanism which yields an anisotropic exchange interaction is a resonant hybridization of the f electrons with the conduction-band electrons, i.e., an interaction of the Coqblin-Schrieffer (CS) type.[6] These hybridization-mediated anisotropic two-ion interactions have been specifically applied to CeX and UX by Cooper and co-workers.[7] Another theoretical model explaining the anomalous magnetic properties in the CeX and UX systems in terms of a mixing of the f states on the cerium or uranium ions with the neighboring anion p orbitals (p-f mixing) has been developed by Takahashi and Kasuya.[8] At present it is not clear which model is more appropriate.

Among the experimental tools, promising progress towards understanding the unusual anisotropy in the CeX and UX compounds is expected from neutron scattering. Diffuse critical neutron scattering (DCNS) and particularly inelastic neutron scattering (INS) are able to provide a very detailed picture of the magnetic anisotropy on a microscopic level. DCNS experiments display the anisotropy of the short-range-ordered spin fluctuations, whereas INS experiments yield direct information about the long-range dynamic spin correlations, from which the size and the nature of both single-ion and two-ion anisotropic interactions can be quantitatively determined.

Some years ago DCNS experiments were performed for

TABLE I. Some properties of the cerium and uranium monopnictides: a is the lattice constant, $(a-c)/c$ is the tetragonal distortion for $T<T_N$, T_N is the ordering temperature, and μ_0 is the ordered magnetic moment.

	a (Å)	Magnetic structure	$(a-c)/c$	T_N (K)	μ_0 (μ_B)
CeP	5.932	AF-I	$<10^{-4}$	8	0.8
CeAs	6.078	AF-I	$<10^{-4}$	8	0.85
CeSb	6.412	6 AF phases ($T<T_N/2$: AF-IA)	$\sim 10^{-3}$	16	2.06
CeBi	6.487	AF-I ($T<T_N/2$: AF-IA)	$\sim 10^{-3}$	25	2.1
UN	4.890	AF-I	$<10^{-4}$	50	0.75
UP	5.589	AF-I	$<10^{-4}$	125	1.8
UAs	5.768	AF-I ($T<T_N/2$: AF-IA)	$<10^{-4}$	126	2.2
USb	6.197	AF-I	$<10^{-4}$	220	2.8

the uranium monopnictides by Lander *et al.*[9] (USb), Sinha *et al.*[10] (UAs), and Holden *et al.*[11] (UN). As a consequence of the anisotropic magnetic interactions only longitudinal short-range-ordered spin fluctuations were observed and their correlation lengths were found to be strongly anisotropic. The same behavior was found for the cerium monopnictides.[12–14] The anisotropy of the correlation lengths continuously decreases from the UX to the CeX systems and towards lighter pnictides, which recently was explained in terms of the CS model for the anisotropic interactions.[15] It should also be noted that an interesting multicritical fluctuation behavior was observed for CeSb.[16,17] Although the phase transition at T_N is first-order, CeSb exhibits critical fluctuations above T_N. However, the short-range ordering of these fluctuations shows AF-I structure, whereas there is no long-range ordering of this type. Above features gave evidence for a competition between bilinear and higher-degree magnetic interaction in CeSb.[17]

In the past there have been many attempts to measure the magnetic excitation spectrum of CeX and UX by INS experiments in order to determine the anomalous coupling mechanism in these systems. Discrete spin waves were observed for CeSb,[14,18,19] CeBi,[19] and USb,[20] whereas for UN (Ref. 21) and UAs (Ref. 22) the magnetic response was found to be spread diffusely in both energy and momentum space. The broad features observed for UN and UAs have been attributed to a fairly large degree of f-electron delocalization. Another puzzling feature was the apparent longitudinal nature of the collective excitation in USb, which has been explained in terms of transverse spin waves in a noncollinear triple-$\mathbf{q}$ structure.[23] Furthermore, the magnetic excitations in CeSb and CeBi could not be consistently interpreted by a simple exchange Hamiltonian. Only for CeBi some calculations of the magnetic excitations within the CS model exist.[24]

In this paper we present new DCNS and INS data for the critical behavior and the magnetic excitations in CeAs, CeSb, and USb. Furthermore, we give a detailed theoretical investigation on the effects of anisotropic exchange interactions on the spin dynamics in these type-I or -IA antiferromagnets.

In Sec. II the theoretical model is described. For the f electrons the electrostatic and the spin-orbit couplings dominate and only the ground-state J multiplets of the magnetic ions are considered, which are split by the crystalline electric field. The anisotropic exchange interactions are described in terms of ion-ion couplings expanded in powers of the spin operators. In our model anisotropic bilinear and isotropic quadrupolar interactions are assumed. A mean-field (MF) calculation in all three spin components yields the static magnetic properties. The spin dynamics then are calculated in the random-phase approximation (RPA) by use of the Green's-function formalism.[25] Including anisotropic interactions, this formalism has already been applied to paramagnets.[26] In the ordered state, however, the RPA formulas strongly depend on the actually realized spin structure and become very complicated. For the AF-I magnets RPA calculations have been performed,[27] but isotropic interactions were assumed. In this paper we give for the first time the RPA formalism for AF-I and related magnetic structures including anisotropic exchange interactions. The above formalism describes both the magnetic excitations and the critical fluctuations and allows a quantitative analysis of the whole spin dynamics as well as the static and critical behavior of the considered magnetic system. Within a two-level model closed expressions for the dispersion curves of the magnetic excitations are given, which may also apply to conventional spin-wave systems. Furthermore, the formalism developed here should be easily adapted to other magnetically ordered states, such as the type-II antiferromagnets, where similar results are expected.

In Sec. III the experimental details are given and in Secs. IV and V the DCNS and INS results for CeAs, CeSb, and USb are presented and discussed. The experiments turn out to provide detailed answers to several key problems. The basically new result of our investigation is the observation of a splitting of the transverse spin-wave excitation into modes with different polarization. This splitting is a direct consequence of the anisotropic exchange interactions present in these systems. For CeAs one of the spin-wave modes shows quadratic dispersion

and nearly zero energy gap at the X points of the Brillouin zone, which has not previously been observed in antiferromagnets. Furthermore, from the observed excitation spectrum for CeAs a collinear single-**q** spin structure emerges in contrast to the triple-**q** configuration postulated by Burlet *et al.*[28] A report on the interesting new excitation behavior observed in CeAs has already been published.[29] For CeSb the magnetic excitations together with the static behavior indicate that in addition to the bilinear exchange interactions strong higher-order magnetic two-ion interactions have to be present, as recently predicted by the p-f mixing model[30] and resulting from DCNS experiments in $Ce_{1-x}(La,Y)_xSb$.[17] Obviously, the often used "axial next-nearest-neighbor Ising" (ANNNI) and related models[31] with competing bilinear interactions alone do not apply to CeSb. Another interesting result is that for CeSb the crystal-field strength was found to be not conserved by going through the phase transition at T_N. The fourth-order crystal-field terms are drastically reduced in the ordered state of CeSb. Finally, the magnetic excitations in USb give strong evidence for localized $5f$ states and predict a very large crystal-field interaction for this compound.

II. THEORY

A. Structural

The antiferromagnetic structures of CeX and UX are characterized by longitudinal magnetic waves with commensurable modulation wave vectors

$$\begin{aligned}\mathbf{q}_0^x&=(2\pi/a)(q_0,0,0)\ ,\\ \mathbf{q}_0^y&=(2\pi/a)(0,q_0,0)\ ,\\ \mathbf{q}_0^z&=(2\pi/a)(0,0,q_0)\ ,\end{aligned}\tag{1}$$

corresponding to a periodic stacking of ferromagnetic (100), (010), or (001) planes, respectively, with the moments perpendicular to the planes. The single components of the magnetic moments $g\mu_B\langle S_i^\alpha\rangle$ at the lattice sites $\mathbf{R}_i$ are the results of a superposition of above longitudinal waves and their higher harmonics

$$\langle S_i^\alpha\rangle=\sum_n c_n e^{in\mathbf{q}_0^\alpha\cdot\mathbf{R}_i}\langle S^\alpha\rangle\quad(0\le nq_0<2)\ ,\tag{2}$$

where the c_n are complex numbers and depend on the actually realized magnetic structure.

The type-I antiferromagnetic structure (AF-I) corresponds to a $+-+-$ stacking of ferromagnetic planes with $q_0=1$. The type-IA antiferromagnetic structure (AF-IA) has a $++--$ stacking and $q_0=\frac{1}{2}$. For the ferromagnetic state (F) we set $q_0=0$. The expectation values for the single spins in the different structures then become

$$\begin{aligned}\langle S_i^\alpha\rangle&=\langle S^\alpha\rangle\quad(F)\\ \langle S_i^\alpha\rangle&=e^{i\mathbf{q}_0^\alpha\cdot\mathbf{R}_i}\langle S^\alpha\rangle\quad(\text{AF-I})\\ \langle S_i^\alpha\rangle&=\tfrac{1}{2}[(1-i)e^{i\mathbf{q}_0^\alpha\cdot\mathbf{R}_i}\\ &\quad+(1+i)e^{-i\mathbf{q}_0^\alpha\cdot\mathbf{R}_i}]\langle S^\alpha\rangle\quad(\text{AF-IA})\ .\end{aligned}\tag{3}$$

Above considerations allow a collinear as well as a noncollinear arrangement of the spins (see Fig. 1). In the collinear case the different $\langle 00q_0\rangle$ waves are separated, giving rise to different domains. For the α domain the α component is the only nonzero spin component and there is a single relevant ordering wave vector $\mathbf{q}_0^\alpha$ (single-**q** structure). This magnetic structure has tetragonal symmetry (P_I4/mnc). In the noncollinear case different longitudinal $\langle 00q_0\rangle$ waves are superposed, so that more than a single $\mathbf{q}_0^\alpha$ is needed to describe the magnetic structure (multi-**q** structure). Of special interest is the cubic configuration ($Pn3$) with an equal population of the three waves parallel to $[q_00]$, $[0q_0]$, and $[00q_0]$ (triple-**q** structure) and the magnetic moments parallel to the $\langle 111\rangle$ directions (Fig. 1.).

Neutron diffraction experiments give identical patterns for the collinear multidomain single-**q** or the noncollinear triple-**q** spin configuration since in Fourier space there is no difference between separation or superposition. An identification of the actually realized spin structure is only possible, if a single-domain state can be guaranteed, e.g., by the application of uniaxial stress or in an external magnetic field. More direct evidence for a single-**q** spin structure, however, is the observation of a tetragonal lattice distortion or a tetragonal symmetry of the magnetic excitations (see Sec. V).

In the following we will always refer to the full nuclear fcc Brillouin zone independent of the realized magnetic structure. In the case of a single-**q** configuration with tetragonal symmetry we will distinguish between the different $\langle 001\rangle$ and $\langle 110\rangle$ directions and denote the symmetry points $(2\pi/a)(100)=X_x$, $(2\pi/a)(010)=X_y$, and $(2\pi/a)(001)=X_z$ (see Fig. 2.).

B. Hamiltonian

To calculate the magnetic behavior of localized f-electron systems a model Hamiltonian is used which includes crystal-field, anisotropic bilinear exchange, and quadrupolar interactions:

$$\mathcal{H}=\mathcal{H}_{\rm CF}+\mathcal{H}_E+\mathcal{H}_Q\ .\tag{4}$$

This operator acts on the $(2J+1)$-fold degenerate ground-state J multiplet of the f electrons. The calculations are performed in the Cartesian coordinate system of the fcc crystal lattice and $[001]||\mathbf{z}$ is the quantization axis.

The crystal-field (CF) potential acts on each ion. The

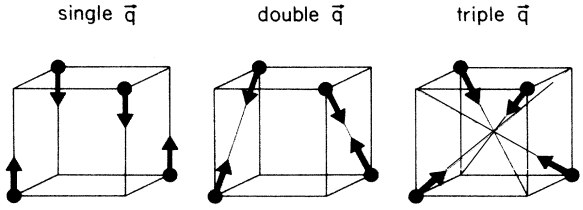

FIG. 1. Different possible spin configurations for the AF-I structure. Only one-quarter of the fcc nuclear cell is displayed.

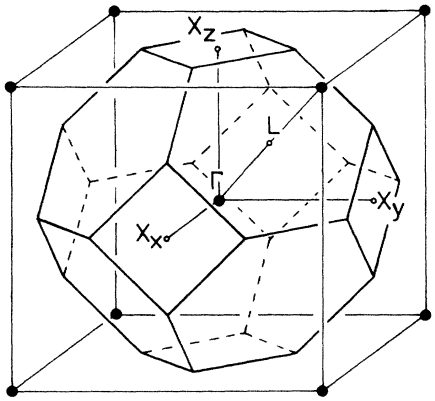

FIG. 2. Brillouin zone of the nuclear fcc lattice. For magnetic structures with tetragonal symmetry the X points are labeled as X_x, X_y, and X_z.

corresponding operator is given by

$$\mathscr{H}_{\mathrm{CF}}=B_4(O_4^0+5O_4^4)+B_6(O_6^0-21O_6^4)\ , \tag{5}$$

where O_n^m are Stevens operators[32] and B_4 and B_6 are effective crystal-field parameters. For Ce^{3+} with $J=\frac{5}{2}$ the sixth-order term vanishes ($B_6=0$). The octahedral crystal field splits the J multiplet of the free ion into different crystal-field levels, namely for Ce^{3+}, Γ_7,Γ_8 and for U^{3+}, $\Gamma_6,2\Gamma_8$.

The anisotropic bilinear exchange interactions are treated as two-ion interactions in a generalized Heisenberg form

$$\mathscr{H}_E=-\sum_{i,j,\alpha,\beta} J_{ij}^{\alpha\beta}S_i^\alpha S_j^\beta\ . \tag{6}$$

S_i^α and S_j^β ($\alpha,\beta=x,y,z$) are components of the total angular momentum operators at the lattice sites $\mathbf{R}_i$ and $\mathbf{R}_j$, respectively, which transform in the usual way as $S^\pm=S^x\pm iS^y$. The $J_{ij}^{\alpha\beta}$ are the most general symmetrically allowed effective bilinear exchange interaction tensors (see the Appendix). The coupling tensors have the same symmetry as the dipolar interactions and transform from one lattice site to the other with the full fcc symmetry. For the ith-neighbor shell the number of coupling parameters reduces to diagonal elements J_i^l and J_i^t with l and t for a predominantly longitudinal or transverse spin configuration with respect to the bonding axis of the ions, respectively, and off-diagonal elements J_i^a.

In close analogy to the bilinear interactions we write for the quadrupolar interactions

$$\mathscr{H}_Q=-\sum_{i,j,\alpha,\beta} K_{ij}'^{\alpha\beta}Q_i^\alpha Q_j^\beta \tag{7}$$

with the quadrupole operators

$$Q_i^\alpha=3(S_i^\alpha)^2-S(S+1)\quad(\alpha=x,y,z)$$

and effective coupling tensors $K_{ij}'^{\alpha\beta}$. We only consider the case of diagonal and isotropic interactions and get

$$\mathscr{H}_Q=-\sum_{i,j} K_{ij}(O_{2_i}^0O_{2_j}^0+3O_{2_i}^2O_{2_j}^2) \tag{8}$$

with

$$\begin{aligned}O_2^0&=3(S^z)^2-S(S+1)\ ,\\ O_2^2&=\tfrac{1}{2}[(S^+)^2+(S^-)^2]\ ,\end{aligned} \tag{9}$$

and effective quadrupolar coupling parameters $K_{ij}=\frac{3}{2}K_{ij}'^{\alpha\alpha}$.

C. Static behavior

1. *Mean-field approximation*

The many-body Hamiltonian Eqs. (6)—(8) may be reduced to a single-ion Hamiltonian by the mean-field approximation (MF). The bilinear exchange and the quadrupolar interactions yield dipolar and quadrupolar molecular fields, respectively, which split the crystal-field levels. We obtain the MF Hamiltonian

$$\begin{aligned}\mathscr{H}_{\mathrm{MF}}=\mathscr{H}_{\mathrm{CF}}&-\sum_{\alpha,\beta}2J^{\alpha\beta}(\mathbf{q}_0^\alpha)\langle S^\alpha\rangle S^\beta\\ &-2K(\mathbf{q}_0^Q)(\langle O_2^0\rangle O_2^0+3\langle O_2^2\rangle O_2^2)\end{aligned} \tag{10}$$

where $J^{\alpha\beta}(\mathbf{q})$ and $K(\mathbf{q})$ are the Fourier-transformed interactions and $\mathbf{q}_0^Q$ is the ordering wave vector of the quadrupole structure. From symmetry (see the Appendix) we have

$$\begin{aligned}&J^{xx}(\mathbf{q}_0^x)=J^{yy}(\mathbf{q}_0^y)=J^{zz}(\mathbf{q}_0^z)=J_0\ ,\\ &J^{\alpha\beta}(\mathbf{q}_0^\alpha)=0\quad(\alpha\neq\beta)\ .\end{aligned} \tag{11}$$

Setting

$$K(\mathbf{q}_0^Q)=K_0\ , \tag{12}$$

we finally arrive at the MF Hamiltonian

$$\begin{aligned}\mathscr{H}_{\mathrm{MF}}=\mathscr{H}_{\mathrm{CF}}&-2J_0(\langle S^x\rangle S^x+\langle S^y\rangle S^y+\langle S^z\rangle S^z)\\ &-2K_0(\langle O_2^0\rangle O_2^0+3\langle O_2^2\rangle O_2^2)\ .\end{aligned} \tag{13}$$

The above Hamiltonian may be solved self-consistently, leading to MF solutions with eigenvalues E_n and eigenvectors $|n\rangle$

$$\mathscr{H}_{\mathrm{MF}}|n\rangle=E_n|n\rangle\quad(n=1,2,\ldots,2S+1)\ . \tag{14}$$

The eigenvectors are linear combinations of the pure angular momentum wave functions

$$|n\rangle=\sum_m a_{nm}|S_m^z\rangle\quad(S_m^z=-S,-S+1,\ldots,S)\ , \tag{15}$$

where, in general, all a_{nm} are nonzero and complex numbers. The expectation value for an operator X is given by

$$\langle X\rangle=\sum_n p_n\langle n|X|n\rangle \tag{16}$$

with Boltzmann occupation numbers

$$p_n=(1/Z)e^{-E_n/kT} \tag{17}$$

and the partition function

$$Z=\sum_n e^{-E_n/kT}\ . \tag{18}$$

2. Single-ion anisotropy

The MF Hamiltonian Eq. (13) always has at least four different types of self-consistent solutions with

$$\begin{aligned}&\text{(a) } \langle S^x\rangle=\langle S^y\rangle=\langle S^z\rangle=0\ ,\\ &\text{(b) } \langle S^x\rangle=\langle S^y\rangle=0,\ \ \langle S^z\rangle\neq 0\ ,\\ &\text{(c) } \langle S^x\rangle=0,\ \ \langle S^y\rangle=\langle S^z\rangle\neq 0\ ,\\ &\text{(d) } \langle S^x\rangle=\langle S^y\rangle=\langle S^z\rangle\neq 0\ .\end{aligned} \tag{19}$$

Case (a) corresponds to the paramagnetic state, whereas for cases (b), (c), and (d) the magnetic moments $\boldsymbol{\mu}=g\mu_B\langle\mathbf{S}\rangle$ are ordered along the cubic symmetry directions [001], [011], and [111], respectively. Consideration of the free energy

$$\begin{aligned}F=&-kT\ln(Z)+J_0(\langle S^x\rangle^2+\langle S^y\rangle^2+\langle S^z\rangle^2)\\&+K_0(\langle O_2^0\rangle^2+3\langle O_2^2\rangle^2)\end{aligned} \tag{20}$$

for all of the cases (a)–(d) yields the energetically lowest state and the easy direction of the moments. The energy difference between states with different spin directions arises from the single-ion anisotropy of the system. This anisotropy is given by the crystal-field and the quadrupolar interactions which both favor a particular spin direction. In cubic symmetry the two-ion anisotropy of the bilinear exchange interactions has no influence on the single-ion anisotropy [compare Eq. (11)].

D. Dynamic behavior

To describe the spin dynamics of localized f-electron systems we use the Green's function formalism in the random-phase approximation (RPA).[25] The formalism treats the collective fluctuations of the system as perturbations to the mean-field state. The noninteracting Green's functions are the single-ion susceptibilities given by the MF eigenstates, and the collective fluctuations are described by the wave-vector-dependent susceptibilities or the spin fluctuations of the single ions due to the perturbation induced by the fluctuations on their neighboring ions.

1. Single-ion susceptibilities

In MF approximation the spin dynamics of a single ion is given by the single-ion susceptibilities[25]

$$\begin{aligned}\chi_0^{\alpha\beta}=&\sum_{\substack{n,m\\E_n\neq E_m}}\frac{\langle n\,|\,S^\alpha\,|\,m\rangle\langle m\,|\,S^\beta\,|\,n\rangle}{E_n-E_m-\omega}(p_m-p_n)\\&+\delta_{\omega,0}\frac{1}{kT}\sum_{\substack{n,m\\E_n=E_m}}[\langle n\,|\,S^\alpha\,|\,m\rangle\langle m\,|\,S^\beta\,|\,n\rangle p_n\\&-\langle S^\alpha\rangle\langle S^\beta\rangle]\ ,\end{aligned} \tag{21}$$

where $E_n-E_m=\Delta_{nm}$ and $\langle n\,|\,S^\alpha\,|\,m\rangle\langle m\,|\,S^\beta\,|\,n\rangle=M_{nm}^{\alpha\beta}$ ($\alpha,\beta=x,y,z,+,-$) are the transition energies and matrix elements between MF eigenstates, respectively.

In the paramagnetic state the single-ion susceptibility tensor reduces to a single paramagnetic susceptibility

$$\begin{aligned}&\chi_0^{xx}(\omega,T)=\chi_0^{yy}(\omega,T)=\chi_0^{zz}(\omega,T)=\chi_0^{P}(\omega,T)\ ,\\&\chi_0^{\alpha\beta}(\omega,T)=0\ \ (\alpha\neq\beta)\ .\end{aligned} \tag{22}$$

In the magnetically ordered state the single-ion susceptibilities depend on the direction of the ordered moment. For $\boldsymbol{\mu}\|[001]$ the MF eigenvectors are real and for symmetry reasons the matrix elements $M_{nm}^{+\,+}$, $M_{nm}^{-\,-}$, and $M_{nm}^{\alpha z}$ ($\alpha\neq z$) vanish. Only a real longitudinal ($\|$), a real transverse ($\perp$), and an imaginary off-diagonal (a) susceptibility remain:

$$\begin{aligned}&\chi_0^{zz}(\omega,T)=\chi_0^{\|}(\omega,T)\ ,\\&\chi_0^{xx}(\omega,T)=\chi_0^{yy}(\omega,T)=\tfrac{1}{4}[\chi_0^{+\,-}(\omega,T)+\chi_0^{-\,+}(\omega,T)]\\&\qquad\qquad=\chi_0^{\perp}(\omega,T)\ ,\\&\chi_0^{xy}(\omega,T)=-\chi_0^{yx}(\omega,T)=(i/4)[\chi_0^{+\,-}(\omega,T)-\chi_0^{-\,+}(\omega,T)]\\&\qquad\qquad=\chi_0^{a}(\omega,T)\ ,\\&\chi_0^{\alpha z}(\omega,T)=0\ \ (\alpha\neq z)\ .\end{aligned} \tag{23}$$

For $\boldsymbol{\mu}\|[111]$ the MF eigenstates are complex and become linear combinations of all pure angular-momentum wave functions. Thus, all matrix elements are nonzero. However, the symmetry reduces the number of different elements of the susceptibility tensor to two, namely a diagonal (d) and an off-diagonal (a) susceptibility

$$\begin{aligned}&\chi_0^{xx}(\omega,T)=\chi_0^{yy}(\omega,T)=\chi_0^{zz}(\omega,T)=\chi_0^{d}(\omega,T)\ ,\\&\chi_0^{xy}(\omega,T)=\chi_0^{yz}(\omega,T)=\chi_0^{zx}(\omega,T)=\chi_0^{a}(\omega,T)\ ,\\&\chi_0^{\alpha\beta}(\omega,T)=(\chi_0^{\beta\alpha})^*(\omega,T)\ .\end{aligned} \tag{24}$$

2. Wave-vector-dependent susceptibilities

Based on the above single-ion susceptibilities the wave-vector-dependent susceptibilities of the coupled spin system may be calculated. In the crystal lattice a perturbation by an external field causes a change of the moments at the single sites, which directly implies a change in the mean-field describing the coupling among the different spins. Thus, an ion at a given lattice site $\mathbf{R}_i$ is influenced not only by the external perturbation, but also by a change in the internal molecular field

$$d\langle S_i^\alpha\rangle=\sum_\beta\chi_{0,i}^{\alpha\beta}(dH_{\mathrm{ex},i}^\beta+dH_{\mathrm{MF},i}^\beta)\ , \tag{25}$$

where the fluctuation in the molecular field is due to the change of the spins on neighboring sites

$$dH_{\mathrm{MF},i}^\beta=\sum_{j,\gamma}2J_{ij}^{\beta\gamma}d\langle S_j^\gamma\rangle\ . \tag{26}$$

In the paramagnetic (P) and the ferromagnetic (F) state the single-ion susceptibilities are equal for all ions in the lattice. However, for the antiferromagnets only the diagonal susceptibilities are equal, whereas the sign of the off-diagonal single-ion susceptibilities changes from sublattice to sublattice. Similar to Eq. (3), we have

$$
\begin{aligned}
&\chi_{0,i}^{\alpha\alpha}=\chi_0^{\alpha\alpha}\ ,\\
&\chi_{0,i}^{\alpha\beta}=\chi_0^{\alpha\beta}\quad (P,F)\\
&\chi_{0,i}^{\alpha\beta}=e^{i\mathbf{q}_0^{\epsilon}\cdot\mathbf{R}_i}\chi_0^{\alpha\beta}\quad (\mathrm{AF-I})\\
&\chi_{0,i}^{\alpha\beta}=\tfrac{1}{2}[(1-i)e^{i\mathbf{q}_0^{\epsilon}\cdot\mathbf{R}_i}+(1+i)e^{-i\mathbf{q}_0^{\epsilon}\cdot\mathbf{R}_i}]\chi_0^{\alpha\beta}\quad (\mathrm{AF-IA})\\
&(\alpha\neq\beta,\ \epsilon\neq\alpha,\ \epsilon\neq\beta,\ \text{and}\ \alpha,\beta,\epsilon=x,y,z)
\end{aligned}
\tag{27}
$$

Taking into account the above site dependence of the single-ion susceptibilities the Fourier transformation of Eq. (25) yields for paramagnets and ferromagnets

$$
d\langle S^{\alpha}(\mathbf{q})\rangle=\sum_{\beta}\chi_0^{\alpha\beta}\left[dH_{\mathrm{ex}}^{\beta}(\mathbf{q})+\sum_{\gamma}2J^{\beta\gamma}(\mathbf{q})d\langle S^{\gamma}(\mathbf{q})\rangle\right],
\tag{28a}
$$

for type-I antiferromagnets

$$
\begin{aligned}
d\langle S^{\alpha}(\mathbf{q})\rangle=&\chi_0^{\alpha\alpha}\left[dH_{\mathrm{ex}}^{\alpha}(\mathbf{q})+\sum_{\gamma}2J^{\alpha\gamma}(\mathbf{q})d\langle S^{\gamma}(\mathbf{q})\rangle\right]\\
&+\sum_{\beta\neq\alpha}\chi_0^{\alpha\beta}\left[dH_{\mathrm{ex}}^{\beta}(\mathbf{q}+\mathbf{q}_0^{\epsilon})+\sum_{\gamma}2J^{\beta\gamma}(\mathbf{q}+\mathbf{q}_0^{\epsilon})d\langle S^{\gamma}(\mathbf{q}+\mathbf{q}_0^{\epsilon})\rangle\right],
\end{aligned}
\tag{28b}
$$

for type-IA antiferromagnets

$$
\begin{aligned}
d\langle S^{\alpha}(\mathbf{q})\rangle=&\chi_0^{\alpha\alpha}\left[dH_{\mathrm{ex}}^{\alpha}(\mathbf{q})+\sum_{\gamma}2J^{\alpha\gamma}(\mathbf{q})d\langle S^{\gamma}(\mathbf{q})\rangle\right]\\
&+\sum_{\beta\neq\alpha}\tfrac{1}{2}(1-i)\chi_0^{\alpha\beta}\left[dH_{\mathrm{ex}}^{\beta}(\mathbf{q}+\mathbf{q}_0^{\epsilon})+\sum_{\gamma}2J^{\beta\gamma}(\mathbf{q}+\mathbf{q}_0^{\epsilon})d\langle S^{\gamma}(\mathbf{q}+\mathbf{q}_0^{\epsilon})\rangle\right]\\
&+\sum_{\beta\neq\alpha}\tfrac{1}{2}(1+i)\chi_0^{\alpha\beta}\left[dH_{\mathrm{ex}}^{\beta}(\mathbf{q}-\mathbf{q}_0^{\epsilon})+\sum_{\gamma}2J^{\beta\gamma}(\mathbf{q}-\mathbf{q}_0^{\epsilon})d\langle S^{\gamma}(\mathbf{q}-\mathbf{q}_0^{\epsilon})\rangle\right].
\end{aligned}
\tag{28c}
$$

We arrive at a system of linear equations coupling the different components x,y,z of spin fluctuations. In the paramagnetic and ferromagnetic state only fluctuations with the same wave vector $\mathbf{q}$ are coupled leading to a 3×3 matrix. In the antiferromagnets the different sublattices may fluctuate in phase or out of phase. Thus, the corresponding system of equations is enlarged to a 6×6 matrix for a single-$\mathbf{q}$ AF-I state or even a 12×12 matrix for triple-$\mathbf{q}$ AF-I and single-$\mathbf{q}$ AF-IA magnets. Solving the system of equations yields the single spin fluctuations $d\langle S^{\alpha}(\mathbf{q})\rangle$ and the wave-vector-dependent susceptibilities $\chi^{\alpha\beta}(\mathbf{q})=d\langle S^{\alpha}(\mathbf{q})\rangle/dH_{\mathrm{ex}}^{\beta}(\mathbf{q})$.

In the paramagnetic and ferromagnetic cases the above system of equations may be written in tensor form yielding the well-known RPA formula

$$
\chi(\mathbf{q})=\chi_0[1+2J(\mathbf{q})\chi(\mathbf{q})]\ .
\tag{29}
$$

With diagonal coupling tensors the system of equations is reduced, and the different components of the wave-vector-dependent susceptibilities partly decouple. This holds especially for some symmetry directions (e.g., $[q00]$, $[0q0]$, $[00q]$, $[0qq]$, $[q0q]$), where $J^{\alpha\beta}(\mathbf{q})=0$ $(\alpha\neq\beta)$. For the resulting wave-vector-dependent susceptibilities we obtain the following.

For paramagnets

$$
\begin{aligned}
&\chi^{\alpha\alpha}(\mathbf{q})=\frac{\chi_0^P}{1-2J^{\alpha\alpha}(\mathbf{q})\chi_0^P}\quad(\alpha=x,y,z)\ ,\\
&\chi^{\alpha\beta}(\mathbf{q})=0\quad(\alpha\neq\beta)\ .
\end{aligned}
\tag{30}
$$

For ferromagnets with $\boldsymbol{\mu}\|[001]$

$$
\begin{aligned}
&\chi^{xx}(\mathbf{q})=\frac{\frac{1}{2}(\chi_0^{+-}+\chi_0^{-+})-J^{yy}(\mathbf{q})\chi_0^{+-}\chi_0^{-+}}{2-[J^{xx}(\mathbf{q})+J^{yy}(\mathbf{q})](\chi_0^{+-}+\chi_0^{-+})+2J^{xx}(\mathbf{q})J^{yy}(\mathbf{q})\chi_0^{+-}\chi_0^{-+}}\ ,\\
&\chi^{yy}(\mathbf{q})=\frac{\frac{1}{2}(\chi_0^{+-}+\chi_0^{-+})-J^{xx}(\mathbf{q})\chi_0^{+-}\chi_0^{-+}}{2-[J^{xx}(\mathbf{q})+J^{yy}(\mathbf{q})](\chi_0^{+-}+\chi_0^{-+})+2J^{xx}(\mathbf{q})J^{yy}(\mathbf{q})\chi_0^{+-}\chi_0^{-+}}\ ,\\
&\chi^{zz}(\mathbf{q})=\frac{\chi_0^{zz}}{1-2J^{zz}(\mathbf{q})\chi_0^{zz}}\ ,\\
&\chi^{xy}(\mathbf{q})=-\chi^{yx}(\mathbf{q})=\frac{i\frac{1}{2}(\chi_0^{+-}-\chi_0^{-+})}{2-[J^{xx}(\mathbf{q})+J^{yy}(\mathbf{q})](\chi_0^{+-}+\chi_0^{-+})+2J^{xx}(\mathbf{q})J^{yy}(\mathbf{q})\chi_0^{+-}\chi_0^{-+}}\ ,\\
&\chi^{xz}(\mathbf{q})=\chi^{yz}(\mathbf{q})=0\ .
\end{aligned}
\tag{31}
$$

For single-**q** type-I antiferromagnets with $\mu||[001]$

$$\chi^{xx}(\mathbf{q})=\frac{\frac{1}{2}(\chi_0^{+-}+\chi_0^{-+})-J^{yy}(\mathbf{q}+\mathbf{q}_0^z)\chi_0^{+-}\chi_0^{-+}}{2-[J^{xx}(\mathbf{q})+J^{yy}(\mathbf{q}+\mathbf{q}_0^z)](\chi_0^{+-}+\chi_0^{-+})+2J^{xx}(\mathbf{q})J^{yy}(\mathbf{q}+\mathbf{q}_0^z)\chi_0^{+-}\chi_0^{-+}},$$

$$\chi^{yy}(\mathbf{q})=\frac{\frac{1}{2}(\chi_0^{+-}+\chi_0^{-+})-J^{xx}(\mathbf{q}+\mathbf{q}_0^z)\chi_0^{+-}\chi_0^{-+}}{2-[J^{yy}(\mathbf{q})+J^{xx}(\mathbf{q}+\mathbf{q}_0^z)](\chi_0^{+-}+\chi_0^{-+})+2J^{yy}(\mathbf{q})J^{xx}(\mathbf{q}+\mathbf{q}_0^z)\chi_0^{+-}\chi_0^{-+}},$$

$$\chi^{zz}(\mathbf{q})=\frac{\chi_0^{zz}}{1-2J^{zz}(\mathbf{q})\chi_0^{zz}}, \tag{32}$$

$$\chi^{\alpha\beta}(\mathbf{q})=0 \quad (\alpha\neq\beta).$$

For single-**q** type-IA antiferromagnets with $\mu||[001]$

$$\begin{aligned}\chi^{xx}(\mathbf{q})=&[\tfrac{1}{2}(\chi_0^{+-}+\chi_0^{-+})-\tfrac{1}{2}(A_1+A_3)\chi_0^{+-}\chi_0^{-+}-\tfrac{1}{8}(A_1+2A_2+A_3)(\chi_0^{+-}+\chi_0^{-+})^2\\&+\tfrac{1}{2}(A_1A_2+A_2A_3+A_3A_1)(\chi_0^{+-}+\chi_0^{-+})\chi_0^{+-}\chi_0^{-+}-A_1A_2A_3(\chi_0^{+-}\chi_0^{-+})^2]\\&\times[2-(A_0+A_1+A_2+A_3)(\chi_0^{+-}+\chi_0^{-+})-(A_0A_1+A_1A_2+A_2A_3+A_3A_0)\chi_0^{+-}\chi_0^{-+}\\&+\tfrac{1}{4}(A_0A_1+A_1A_2+A_2A_3+A_3A_0+2A_0A_2+2A_1A_3)(\chi_0^{+-}+\chi_0^{-+})^2\\&-(A_0A_1A_2+A_1A_2A_3+A_2A_3A_0+A_3A_0A_1)(\chi_0^{+-}+\chi_0^{-+})\chi_0^{+-}\chi_0^{-+}+2A_0A_1A_2A_3(\chi_0^{+-}\chi_0^{-+})^2]^{-1}\end{aligned} \tag{33}$$

with

$$A_0=J^{xx}(\mathbf{q}),\quad A_1=J^{yy}(\mathbf{q}+\mathbf{q}_0^z),$$

$$A_2=J^{xx}(\mathbf{q}+2\mathbf{q}_0^z),\quad A_3=J^{yy}(\mathbf{q}+3\mathbf{q}_0^z),$$

$\chi^{yy}(\mathbf{q})$ analogous to $\chi^{xx}(\mathbf{q})$ with x and y interchanged,

$$\chi^{zz}(\mathbf{q})=\frac{\chi_0^{zz}}{1-2J^{zz}(\mathbf{q})\chi_0^{zz}},$$

$$\chi^{\alpha\beta}(\mathbf{q})=0 \quad (\alpha\neq\beta).$$

For triple-**q** type-I antiferromagnets with $\mu||[111]$

$$\begin{aligned}\chi^{xx}(\mathbf{q})=&\{\chi_0^d-2(A_1+A_2)(|\chi_0^d|^2-|\chi_0^a|^2)+4A_1A_2[(\chi_0^d)^3-3\chi_0^d|\chi_0^a|^2+(\chi_0^a)^3+(\chi_0^{a*})^3]\}\\&\times\{1-2(A_0+A_1+A_2)\chi_0^d+4(A_0A_1+A_1A_2+A_2A_0)(|\chi_0^d|^2-|\chi_0^a|^2)\\&-8A_1A_2A_3[(\chi_0^d)^3-3\chi_0^d|\chi_0^a|^2+(\chi_0^a)^3+(\chi_0^{a*})^3]\}^{-1}\end{aligned} \tag{34}$$

with

$$A_0=J^{xx}(\mathbf{q}),\quad A_1=J^{yy}(\mathbf{q}+\mathbf{q}_0^z),\quad A_2=J^{zz}(\mathbf{q}+\mathbf{q}_0^y),$$

$\chi^{yy}(\mathbf{q})$ and $\chi^{zz}(\mathbf{q})$ analogous with cyclic permutation of x,y,z and

$$\chi^{\alpha\beta}(\mathbf{q})=0 \quad (\alpha\neq\beta).$$

In general, the off-diagonal elements of the Fourier-transformed exchange interaction tensor couple all components of the spin fluctuations, and the full system of equations (28) has to be solved. The resulting expressions for the particular susceptibilities become very complicated and are not explicitly reproduced here.

3. *Magnetic excitations*

The magnetic excitations (crystal-field excitations, magnons or spin waves) of a spin system are given by the poles of the wave-vector-dependent susceptibilities [e.g., Eqs. (30)–(34)]. In a crystal the resonances $\omega=\Delta_{nm}$ of the single-ion susceptibilities [Eq. (21)] become dependent on the wave vector **q** by the exchange interactions leading to dispersion curves $\omega(\mathbf{q})$. The intensities $I(\mathbf{q})$ of the excitations are proportional to the residue of the corresponding poles. In general, the dispersion curves of the magnetic excitations and the intensities have to be calculated numerically. However, for a two-level system simple expressions for $\omega(\mathbf{q})$ and $I(\mathbf{q})$ may be obtained as shown below.

In the paramagnetic state only the crystal field acts on the single ion and splits the J multiplet of the free ion into crystal-field levels. As a simple example, for Ce^{3+} we get a doublet Γ_7 and a quartet Γ_8 separated by $\Delta_{CF}=360B_4$. The paramagnetic single-ion susceptibility Eq. (22) then becomes

$$\chi_0^P(\omega,T)=\tfrac{80}{9}\frac{\Delta_{CF}}{\Delta_{CF}^2-\omega^2}(p_{\Gamma_7}-p_{\Gamma_8}), \tag{35}$$

and with diagonal exchange interactions we obtain from Eq. (30) for the dispersion and the intensity of the crystal-field excitation

$$\begin{aligned}\omega^{\alpha\alpha}(\mathbf{q})&=[\Delta_{CF}^2-\tfrac{160}{9}J^{\alpha\alpha}(\mathbf{q})\Delta_{CF}(p_{\Gamma_7}-p_{\Gamma_8})]^{1/2},\\I^{\alpha\alpha}(\mathbf{q})&=\tfrac{80}{9}\Delta_{CF}(p_{\Gamma_7}-p_{\Gamma_8}) \quad (\alpha=x,y,z),\end{aligned} \tag{36}$$

The anisotropic exchange interactions split the crystal-field excitation into three modes with different polariza-

tions which may be partly degenerate along symmetry directions.

In the magnetically ordered state the degeneracy of the crystal-field levels is completely lifted by the molecular fields. Each transition between two MF eigenstates leads to at least one dispersion curve. If the molecular fields are strong compared to the crystal field, we get nearly pure Zeeman levels $|S\rangle$, $|S-1\rangle, \ldots, |-S\rangle$. Then at $T\sim 0$ the ordered magnetic moment has almost the value of the free ion, and the magnetic excitations correspond to conventional transverse spin waves. In the RPA formalism only the two lowest-lying levels become relevant, and the system is well described by a two-level model with a transverse transition. On the other hand, for a Kramer's ion a strong crystal field may create a well-isolated ground-state doublet which forms an effective $S=\frac{1}{2}$ system, and again a two-level model with a transverse transition applies.

For $\boldsymbol{\mu}\|[001]$ and $T\sim 0$ the relevant single-ion susceptibilities [Eqs. (21) and (23)] for the two-level model with a transverse transition are

$$\chi_0^{+-}(\omega)=\frac{M}{\Delta-\omega},\ \chi_0^{-+}(\omega)=\frac{M}{\Delta+\omega}\ , \tag{37}$$

where Δ is the energy splitting of the two levels, and M is the transition matrix element. Then only xx and yy excitations exist, and with $J^{\alpha\beta}(\mathbf{q})=0$ $(\alpha\neq\beta)$ we obtain the following.

For ferromagnets

$$\begin{aligned}
&\omega^{xx}(\mathbf{q})=\omega^{yy}(\mathbf{q})\\
&\qquad=\{[\Delta-J^{xx}(\mathbf{q})M][\Delta-J^{yy}(\mathbf{q})M]\}^{1/2}\ ,\\
&I^{xx}(\mathbf{q})=[M\Delta-J^{yy}(\mathbf{q})M^2]/2\omega^{xx}(\mathbf{q})\ ,\\
&I^{yy}(\mathbf{q})=[M\Delta-J^{xx}(\mathbf{q})M^2]/2\omega^{yy}(\mathbf{q})\ .
\end{aligned} \tag{38}$$

For single-$\mathbf{q}$ type-I antiferromagnets

$$\begin{aligned}
&\omega^{xx}(\mathbf{q})=\{[\Delta-J^{xx}(\mathbf{q})M][\Delta-J^{yy}(\mathbf{q}+\mathbf{q}_0^z)M]\}^{1/2}\ ,\\
&\omega^{yy}(\mathbf{q})=\{[\Delta-J^{xx}(\mathbf{q}+\mathbf{q}_0^z)M][\Delta-J^{yy}(\mathbf{q})M]\}^{1/2}\\
&I^{xx}(\mathbf{q})=[M\Delta-J^{yy}(\mathbf{q}+\mathbf{q}_0^z)M^2]/2\omega^{xx}(\mathbf{q})\ ,\\
&I^{yy}(\mathbf{q})=[M\Delta-J^{xx}(\mathbf{q}+\mathbf{q}_0^z)M^2]/2\omega^{yy}(\mathbf{q})\ .
\end{aligned} \tag{39}$$

For single-$\mathbf{q}$ type-IA antiferromagnets

$$\begin{aligned}
&\omega_{\pm}^{xx}(\mathbf{q})=(\Omega_1^{xx}\pm\Omega_2^{xx})^{1/2}\ ,\\
&\Omega_1^{xx}=[\Delta-\tfrac{1}{2}(A_0+A_2)M][\Delta-\tfrac{1}{2}(A_1+A_3)M]\ ,\\
&\Omega_2^{xx}=[(\Omega_1^{xx})^2-(\Delta-A_0M)(\Delta-A_1M)(\Delta-A_2M)(\Delta-A_3M)]^{1/2}\ ,\\
&I_{\pm}^{xx}(\mathbf{q})=\frac{[M\Delta-\frac{1}{2}(A_1+A_3)M^2][\omega_{\pm}^{xx}(\mathbf{q})]^2-M(\Delta-A_1M)(\Delta-A_2M)(\Delta-A_3M)}{4\{[\omega_{\pm}^{xx}(\mathbf{q})]^2-[\omega_{\mp}^{xx}(\mathbf{q})]^2\}\omega_{\pm}^{xx}(\mathbf{q})}\ ,
\end{aligned} \tag{40}$$

with

$$\begin{aligned}
&A_0=J^{xx}(\mathbf{q}),\quad A_1=J^{yy}(\mathbf{q}+\mathbf{q}_0^z)\ ,\\
&A_2=J^{xx}(\mathbf{q}+2\mathbf{q}_0^z),\quad A_3=J^{yy}(\mathbf{q}+3\mathbf{q}_0^z)
\end{aligned}$$

and $\omega_{\pm}^{yy}(\mathbf{q})$ and $I_{\pm}^{yy}(\mathbf{q})$ analogous with x and y interchanged.

For $\boldsymbol{\mu}\|[111]$ the matrix elements of a transverse transition (here transverse means with respect to [111]) are from symmetry

$$\begin{aligned}
&M^{xx}=M^{yy}=M^{zz}=M\ ,\\
&M^{xy}=M^{yz}=M^{zx}=(-\tfrac{1}{2}+i\sqrt{3}/2)M\ ,
\end{aligned} \tag{41}$$

and for the two-level model the single-ion susceptibilities [Eq. (24)] at $T\sim 0$ become

$$\begin{aligned}
&\chi_0^d(\omega)=\frac{2M\Delta}{\Delta^2-\omega^2}\ ,\\
&\chi_0^a(\omega)=\frac{-M\Delta+i\sqrt{3}M\omega}{\Delta^2-\omega^2}\ .
\end{aligned} \tag{42}$$

In triple-$\mathbf{q}$ structures a transverse transition leads to a response in the xx, yy, and zz components of the susceptibility. For the magnetic excitations in the AF-I triple-$\mathbf{q}$ state with $J^{\alpha\beta}(\mathbf{q})=0$ $(\alpha\neq\beta)$ we get

$$\begin{aligned}
&\omega^{\alpha\alpha}(\mathbf{q})=[\Delta^2-4(A_0+A_1+A_2)M\Delta\\
&\qquad+12(A_0A_1+A_1A_2+A_2A_0)M^2]^{1/2}\ ,\\
&I^{\alpha\alpha}(\mathbf{q})=[M\Delta-3(A_1+A_2)M^2]/\omega^{\alpha\alpha}(\mathbf{q})\ ,
\end{aligned} \tag{43}$$

where for $\alpha=x$

$$A_0=J^{xx}(\mathbf{q}),\quad A_1=J^{yy}(\mathbf{q}+\mathbf{q}_0^z),\quad A_2=J^{zz}(\mathbf{q}+\mathbf{q}_0^y)\ ,$$

for $\alpha=y$

$$A_0=J^{yy}(\mathbf{q}),\quad A_1=J^{zz}(\mathbf{q}+\mathbf{q}_0^x),\quad A_2=J^{xx}(\mathbf{q}+\mathbf{q}_0^z)\ ,$$

for $\alpha=z$

$$A_0=J^{zz}(\mathbf{q}),\quad A_1=J^{xx}(\mathbf{q}+\mathbf{q}_0^y),\quad A_2=J^{yy}(\mathbf{q}+\mathbf{q}_0^x)\ .$$

From the dispersion behavior obtained for the two-level systems given above, we conclude that each MF transition leads to only one dispersion curve in ferromagnets, whereas in antiferromagnets the anisotropic exchange interactions split the transverse excitations into modes with different polarization.

Up to now we only considered the case of diagonal exchange interactions. Within the two-level model it may be shown that in a single-$\mathbf{q}$ AF-I state the off-diagonal elements of the interaction tensor yield an additional cou-

pling of the xx and yy fluctuations, which splits the MF transitions into different modes also along symmetry directions where they are degenerate in the diagonal case (e.g., $[qqq]$). We get

$$\omega^{xx}(\mathbf{q})=(\Omega_1-|\Omega_2|)^{1/2}$$
$$\omega^{yy}(\mathbf{q})=(\Omega_1+|\Omega_2|)^{1/2}, \tag{44}$$

with

$$\Omega_1=\Delta^2-\tfrac{1}{2}(A_0+A_1+A_2+A_3)M\Delta+\tfrac{1}{2}(A_0A_3+A_1A_2-2B_0B_1)M^2,$$
$$\Omega_2=\{[\tfrac{1}{2}(A_0-A_1-A_2+A_3)M\Delta-\tfrac{1}{2}(A_0A_3-A_1A_2)M^2]^2+(B_0-B_1)^2M^2\Delta^2$$
$$+(A_0B_1+A_1B_0+A_2B_1+A_3B_0)(B_0-B_1)M^3\Delta+(A_0A_2B_1^2-A_0A_3B_0B_1-A_1A_2B_0B_1+A_1A_3B_0^2)M^4\}^{1/2},$$
$$A_0=J^{xx}(\mathbf{q}),\quad A_1=J^{xx}(\mathbf{q}+\mathbf{q}_0^z),\quad A_2=J^{yy}(\mathbf{q}),\quad A_3=J^{yy}(\mathbf{q}+\mathbf{q}_0^z),$$
$$B_0=J^{xy}(\mathbf{q}),\quad B_1=J^{xy}(\mathbf{q}+\mathbf{q}_0^z).$$

A similar splitting may also be expected for AF-IA and triple-$\mathbf{q}$ magnets.

The magnetic excitations provide detailed information on all the parameters of the model Hamiltonian considered. The crystal-field transitions in the paramagnetic state determine B_4 and B_6, and the MF transitions in the ordered state yield, in addition to the crystal-field parameters, the molecular-field parameters J_0 and K_0. The dispersion behavior of the single transitions give the wave-vector dependence of the bilinear exchange interactions which is defined by the different two-ion couplings.

4. *Quasistatic fluctuations*

The quasistatic short-range ordered spin fluctuations become important in the critical temperature region of a second-order phase transition and are therefore often called critical fluctuations. Following the "fluctuation-dissipation theorem," they are described in the quasistatic approximation by the static or elastic part of the wave-vector-dependent susceptibilities.

In the paramagnetic state the wave-vector-dependent susceptibilities along $[q00]$, $[0q0]$, and $[00q]$ where $J^{\alpha\beta}(\mathbf{q})=0$ $(\alpha\neq\beta)$ become [Eq. (30)]

$$\chi^{\alpha\alpha}(\mathbf{q},\omega=0)=\frac{\chi_0^P(\omega=0)}{1-2J^{\alpha\alpha}(\mathbf{q})\chi_0^P(\omega=0)}. \tag{45}$$

The single susceptibilities $\chi^{\alpha\alpha}(\mathbf{q},\omega=0)$ are directly related to the corresponding exchange interactions $J^{\alpha\alpha}(\mathbf{q})$ and show the same symmetry. The fluctuations $\chi^{\alpha\alpha}(\mathbf{q},\omega=0)$ are peaking at the ordering wave vector $\mathbf{q}_0^\alpha$ where the couplings $J^{\alpha\alpha}(\mathbf{q})$ reach their maxima. By expanding the $J^{\alpha\alpha}(\mathbf{q})$ around $\mathbf{q}_0^\alpha$ we get the famous Ornstein-Zernike formula which suggests that the susceptibilities become Lorentzians in $\mathbf{q}$ space with half-widths proportional to the quadratic term in the above expansion. The position and half-widths of the Lorentzians define the structure and mean inverse correlation lengths of the fluctuations, respectively. The anisotropic exchange interactions lead to two different inverse correlation lengths $\kappa_{||}$ and $\kappa_\perp$, longitudinal and transverse to the spin direction. We get

$$\chi^{\alpha\alpha}(\mathbf{q}_0^\alpha+\mathbf{q}_{||},\omega=0)\sim 1/(\kappa_{||}^2+q_{||}^2),$$
$$\chi^{\alpha\alpha}(\mathbf{q}_0^\alpha+\mathbf{q}_\perp,\omega=0)\sim 1/(\kappa_\perp^2+q_\perp^2). \tag{46}$$

For AF-I fluctuations with $q_0=1$ the anisotropy of the inverse correlation lengths $\kappa_{||}/\kappa_\perp$ becomes

$$\frac{\kappa_{||}}{\kappa_\perp}=\left|\frac{-\frac{1}{2}J_1^l+\frac{1}{2}J_1^t+J_2^t+J_3^l-5J_3^t+2J_4^l+2J_4^t+\cdots}{-J_1^l+J_2^l+4J_3^l-2J_3^t+4J_4^l+\cdots}\right|^{1/2}. \tag{47}$$

Obviously the anisotropy of the quasistatic fluctuations reflects the exchange anisotropies to the different neighbors in an integral manner.

The information on the exchange interactions given by the quasistatic fluctuations is limited. One only finds the wave vector for which the exchange couplings reach a maximum as well as the behavior of the Fourier-transformed coupling tensor in the vicinity of that maximum. Concerning the anisotropy of the exchange interactions only qualitative statements are possible.

E. Quadrupolar effects

In the above calculations of the spin dynamics the quadrupolar interactions entered only as the single-ion parameter K_0. In fact, the effects of a possible tetragonal lattice distortion by magnetoelastic interactions are correctly described by the quadrupolar single-ion Hamiltonian. However, the two-ion quadrupolar interactions exhibit a wave-vector dependence and will influence the dispersion behavior of the system. Usually in the ordered state there is an internal coupling of the spin and quadrupolar moments of the single ion, and the spin and quadrupolar fluctuations get mixed. For isotropic interactions detailed calculations along this line have been performed.[33] With anisotropic exchange interactions $J^{\alpha\beta}(\mathbf{q})$ and quadrupolar interactions $K(\mathbf{q})$ the systems of coupled equations [Eq. (28)], however, become very large and complicated. Here the variations of $K(\mathbf{q})$ as a function of $\mathbf{q}$ are assumed to be small enough that their influence on the dispersion behavior may be neglected.

F. Neutron cross sections

The wave-vector-dependent spin susceptibilities may be directly measured by neutron scattering. In contrast to other experimental methods neutron scattering allows us to measure the susceptibilities in the whole reciprocal space.

Inelastic neutron scattering experiments (INS) yield the magnetic excitations or the inelastic part of the wave-vector-dependent susceptibilities. The cross section is[34]

$$\frac{\partial\sigma}{\partial\Omega\,\partial\omega}\sim(1-e^{-\hbar\omega/kT})^{-1}F^2(\mathbf{Q})\times\sum_{\alpha,\beta}(\delta_{\alpha\beta}-Q^\alpha Q^\beta/Q^2)\,\mathrm{Im}\chi^{\alpha\beta}(\mathbf{q},\omega,T)\,, \tag{48}$$

where $\mathbf{Q}=\mathbf{q}+\tau$ is the scattering vector and τ is a reciprocal-lattice vector. $F(\mathbf{Q})$ is the magnetic form factor. With the use of the polarization factor $(\delta_{\alpha\beta}-Q^\alpha Q^\beta/Q^2)$ neutrons can only couple to spin fluctuations perpendicular to the scattering vector $\mathbf{Q}$, which allow us to determine the single components of the susceptibility tensor by measuring in different Brillouin zones. In a magnetically ordered crystal different equivalent domains usually coexist and a superposition of the corresponding susceptibilities is observed. The scattering contributions of the individual domains may be obtained by forcing the crystal to form a magnetic single domain state by application of external fields.

The elastic scattering at the short-range-ordered spin fluctuations is called diffuse critical neutron scattering (DCNS). In the quasistatic approximation the cross section is[34]

$$\frac{\partial\sigma}{\partial\Omega}\sim F^2(\mathbf{Q})\sum_{\alpha,\beta}(\delta_{\alpha\beta}-Q^\alpha Q^\beta/Q^2)kT\chi^{\alpha\beta}(\mathbf{q},\omega=0,T)\,. \tag{49}$$

III. EXPERIMENT

The experiments were performed on single crystals of CeAs ($\sim$0.3 cm^3), CeSb ($\sim$0.1 cm^3), and USb ($\sim$0.7 cm^3) which were grown by the recrystallization method[35] by Vogt and Mattenberger at the Eidgenössische Technische Hochschule Zürich-Hönggerberg (Zurich, Switzerland).

Most of the INS measurements were carried out on the triple-axis spectrometers at the reactor Saphir at Würenlingen. To gain intensity doubly bent monochromator and horizontally bent analyzer systems were used, both made of pyrolitic graphite. The measurements were performed in the neutron energy-loss configuration with the analyzer energy kept fixed at 13.7 or 14.9 meV and pyrolitic graphite as the higher-order filter. The high-resolution INS experiments on CeAs were carried out at Risø National Laboratory on the triple-axis spectrometer TAS7 which is installed at a neutron guide connected to a cold H_2 source. Then a 5.0- or 2.6-meV analyzer energy and a Be filter were used.

The DCNS experiments were performed on a double-axis spectrometer at Würenlingen. The detector could be moved out of the scattering plane allowing $\mathbf{q}$ scans in all three directions of the reciprocal space. The neutron energy was 13.7 meV and a 10-cm-thick pyrolitic graphite filter removed the higher-order contamination of the beam. Cryostats and closed-cycle He refrigerators were used as cooling systems. For measurements with an external magnetic field the sample was mounted in a 45-kOe superconducting magnet.

IV. ANISOTROPIC CORRELATION BEHAVIOR ABOVE T_N

DCNS experiments performed for UX (Refs. 9–11) and CeX (Refs. 12–14 and 17) nicely demonstrated the presence of anisotropic bilinear exchange interactions. For all these compounds (with the exception of UAs) DCNS shows diffuse Lorentzian peaks at the AF-I centers or the X points of the Brillouin zone. The DCNS intensity is seen near {110} but not at {001}, which means that according to the polarization factor in the neutron cross section Eq. (49) the $\alpha\alpha$ fluctuations in the X_α points are much larger than the fluctuations in the other spin components

$$\chi^{\alpha\alpha}(X_\alpha,\omega=0)\gg\chi^{\beta\beta}(X_\alpha,\omega=0)\quad(\alpha\neq\beta)\,.$$

Using Eq. (45), it directly follows that the exchange couplings $J^{\alpha\alpha}(\mathbf{q})$ reach a maximum at the X_α points and that the interactions are strongly anisotropic

$$J^{\alpha\alpha}(X_\alpha)\gg J^{\beta\beta}(X_\alpha)\quad(\alpha\neq\beta)\,.$$

The observed DCNS intensity distributions are anisotropic in $\mathbf{q}$ space. The contours of equal intensity are cigarlike as schematically is shown in Fig. 3, with the exception of CeAs which exhibits a lenslike intensity distribution. Typical DCNS scans for CeSb and CeAs are shown in Fig. 4. The half-widths of the DCNS peaks directly yield the inverse correlation lengths $\kappa_\parallel$ and $\kappa_\perp$, parallel and perpendicular to the spin direction. The anisotropy of the correlation lengths $\kappa_\parallel/\kappa_\perp$ turned out to be almost temperature independent:

$$\kappa_\parallel/\kappa_\perp=0.6\pm0.1\quad(\mathrm{CeAs})$$

$$\kappa_\parallel/\kappa_\perp=1.8\pm0.3\quad(\mathrm{CeSb})$$

$$\kappa_\parallel/\kappa_\perp=5.0\pm0.5\quad(\mathrm{USb})\,.$$

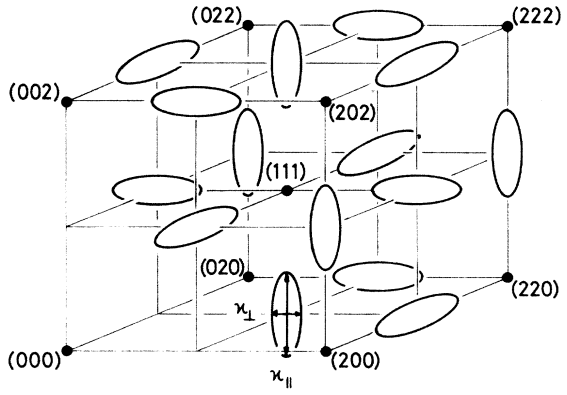

FIG. 3. Situation in the reciprocal space of CeX and UX for $T>T_N$: diffuse neutron scattering is observed in the AF-I centers with anisotropic inverse correlation lengths $\kappa_\parallel$ and $\kappa_\perp$.

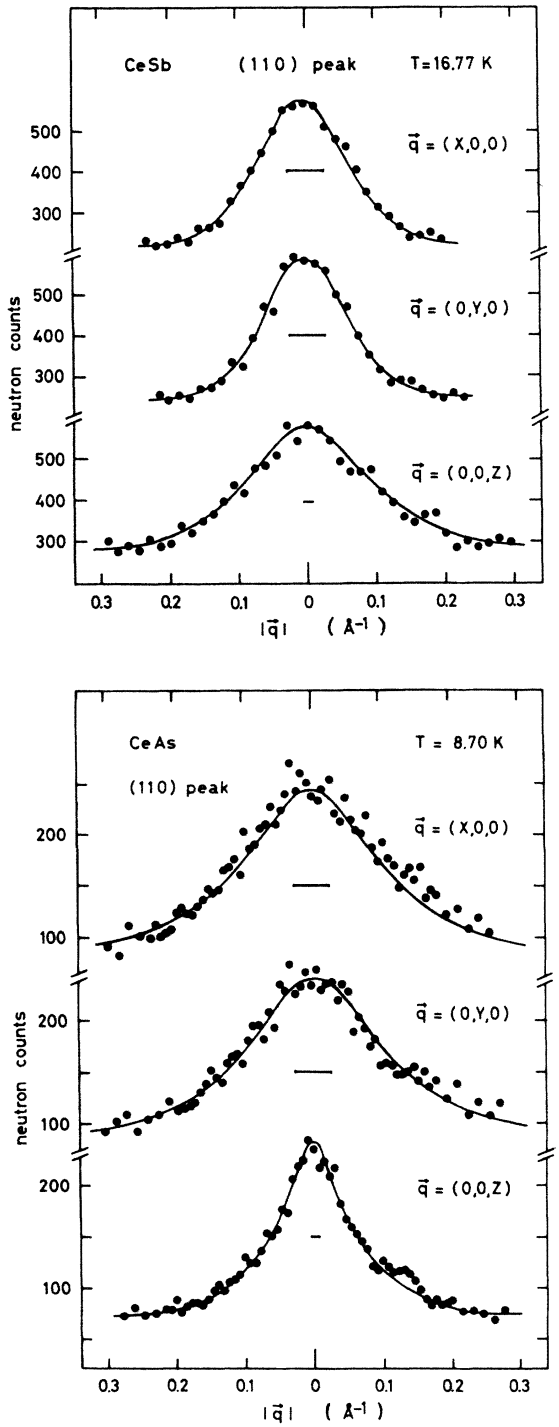

FIG. 4. DCNS intensity distributions in CeSb and CeAs: **q** scans along the cubic $\langle 00q \rangle$ directions through (110) show Lorentzian peaks with anisotropic half-widths. The experimental resolution is indicated by the horizontal bars.

The last value is from Ref. 9. The anisotropic correlation behavior above T_N is a direct evidence for anisotropic magnetic interactions. For CeSb and USb the couplings within the ferromagnetic (001) planes are stronger than the interplanar couplings, whereas for CeAs the ratio of the coupling strengths is reversed. Recently, Kioussis and Cooper[15] could explain above change in the anisotropic correlation behavior in terms of the CS model with hybridization-mediated two-ion interactions.

V. MAGNETIC EXCITATIONS

A. CeAs, AF-I single-q structure

CeAs orders below $T_N \sim 8$ K in a AF-I structure. In the paramagnetic state at $T=9$ K, INS experiments were performed along the symmetry directions $[00q]$, $[qq0]$, and $[qqq]$. Consistent to earlier powder measurements of Heer *et al.*[36] a crystal-field transition with $\Delta_{CF} \sim 13$ meV was found. The lowest-lying J multiplet of the Ce^{3+} ion is split into the doublet Γ_7 as the ground state and the quartet Γ_8 as the excited state. The observed crystal-field transition shows a slight dispersion [Fig. 5(a)] and is split into two modes at the X points as a consequence of anisotropic magnetic interactions. At (003) only the energetically higher mode is observed, whereas at (110) both modes appear (Fig. 6). Because of the polarization factor in the neutron cross section at (003) one measures only χ^{xx} and χ^{yy}, which are both equal by symmetry. However, at (110) the xx and yy excitations have half intensity, and in addition the zz excitation, which has a lower energy, appears. The magnetic excitations $\omega^{\alpha\alpha}(\mathbf{q})$ in the paramagnetic state [Eq. (36)] are directly related to the corresponding interactions $J^{\alpha\alpha}(\mathbf{q})$, and we get

$$J^{zz}(X_z) \gg J^{xx}(X_z) = J^{yy}(X_z) ,$$

which is consistent with the DCNS experiments. The dispersion curves of the crystal-field excitation may be calculated by Eq. (36) which reliably defines the crystal-field parameter B_4.

Since the crystal-field splitting of ~ 160 K is very large compared to the ordering temperature of ~ 8 K, the magnetic behavior of CeAs is dominated by the well-isolated ground-state doublet Γ_7. In the ordered state the doublet is split by the molecular field. The transitions within the doublet were measured by INS experiments with cold neutrons. Figure 7 shows typical scans and in Fig. 5(b) the observed energies of the excitations at $T=4.2$ K for wave vectors along the symmetry directions of the fcc Brillouin zone are summarized.

CeAs exhibits a fundamental new magnetic excitation behavior. At the X points the dispersion is quadratic with a nearly zero energy gap of ~ 0.03 meV (Fig. 8). This is in contrast to the linear dispersion which is generally observed for antiferromagnetic magnons.

Similar to the crystal-field excitation the doublet transition is split into two modes at the X points. The lower-lying mode is observed near (110) but not near (001) (Fig. 7), indicating an apparent longitudinal character of the excitation. Taking into account the multidomain structure of the crystal, however, this mode clearly corresponds to a transverse spin-wave excitation as shown below.

By application of a magnetic field of 21 kOe along [110] (or 40 kOe along [210]) in CeAs a single-domain single-**q** AF-I state with $\mathbf{q}_0=(2\pi/a)(0,0,1)$ (z domain) is obtained. Then the excitations of wave vector $\mathbf{q} \| [00q]$, perpendicular to the ferromagnetic planes, show normal

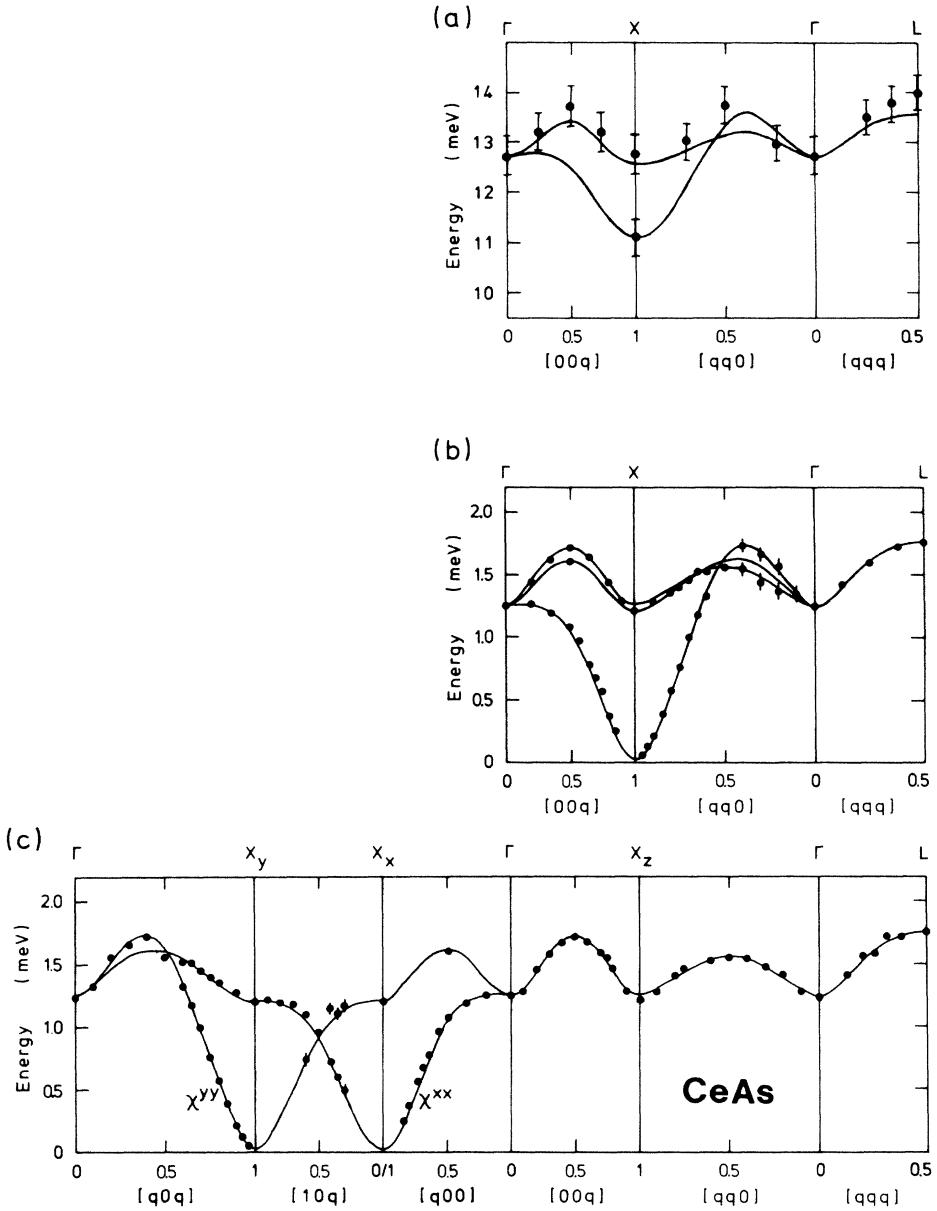

FIG. 5. Dispersion curves of the magnetic excitations in CeAs: (a) crystal-field transition $\Gamma_7 \rightarrow \Gamma_8$ in the paramagnetic state at $T=9$ K; (b) spin waves in the multidomain AF-I single-**q** state at $T=4.2$ K and $\mathbf{H}=\mathbf{0}$; (c) spin waves in the AF-I z domain at $T=4.2$ K. The solid lines represent the theoretical dispersion curves calculated with the parameters in Table II.

spin-wave behavior and a large energy gap of 1.2 meV at the X point (Fig. 7). But for $\mathbf{q}\|[q00]$ and $\mathbf{q}\|[0q0]$, within the (001) planes, the peculiar branch with nearly zero energy at the X_x and X_y points is observed [Figs. 7 and 5(c)]. Figure 5(c) shows the excitation spectrum of the z domain again within the full nuclear Brillouin zone, but with respect to the tetragonal symmetry of the single-**q** AF-I structure.

The intensity behavior of the excitations in the single-domain state ($H \neq 0$) yields the polarizations of the different branches. The neutron intensities near (001) and (110) (Fig. 7) indicate a transverse character of the excitations. At (001) the polarization factor allows only transverse excitations (χ^{xx} and χ^{yy}), whereas at (110) the same transverse excitations appear with half the intensity, but it is also possible that longitudinal excitations could be observed. The excitation spectra for wave vectors along the symmetry direction $[10q]$ from $(120)=X_x$ to $(121)=X_y$ (Fig. 9) finally allow the determination of the polarization of the two split transverse branches. There the polarization factor is ~ 0.8 for the xx excitations and ~ 0.2 for the yy excitations. Thus the more intense excitation with the energy minimum at the X_x point has xx polarization, and the weaker mode with the energy minimum at the X_y point has yy polarization.

Obviously the zero-field spectrum in CeAs [Fig. 5(b)] can be considered as a superposition of the appropriate spectra [Fig. 5(c)] of the three equivalent $\langle 001 \rangle$ domains,

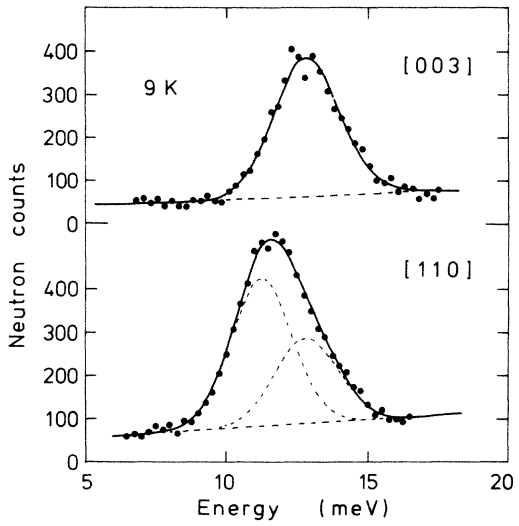

FIG. 6. INS spectra of the crystal-field excitation $\Gamma_7 \rightarrow \Gamma_8$ in the paramagnetic state of CeAs indicating a splitting of the transition at the X points.

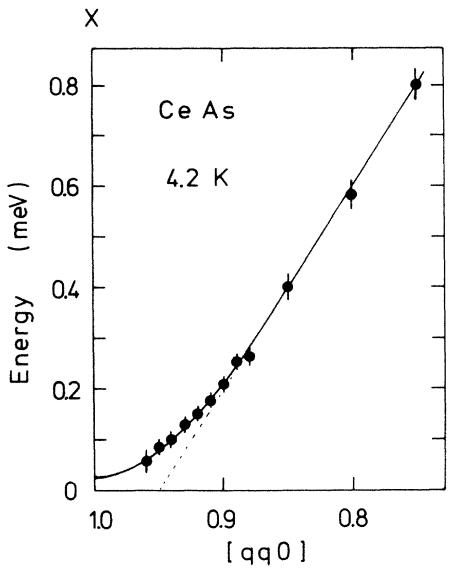

FIG. 8. Quadratic dispersion for the spin waves at the X points of CeAs at $T=4.2$ K.

corresponding to a multidomain AF-I state. In particular, the $[00q]$ direction of Fig. 5(b) is just a superposition of the $[00q]$ and $[q00]$ directions in Fig. 5(c). The observation of two higher-energy excitations along $[00q]$ in zero field directly demonstrates that the spins in CeAs are ordered in a single-**q** structure. The tetragonal symmetry of the single-**q** structure allows different excitation energies for wave vectors within or perpendicular to the ferromagnetic planes, both of which can be observed simultaneously in the multidomain crystal. For the triple-**q** structure with cubic symmetry the $[q00]$, $[0q0]$, and $[00q]$ directions are equivalent and only a single higher-energy mode is expected. A comparison of the INS spectra for the single- and multidomain crystal shows no change in the excitation peak at (002), but a significant broadening of

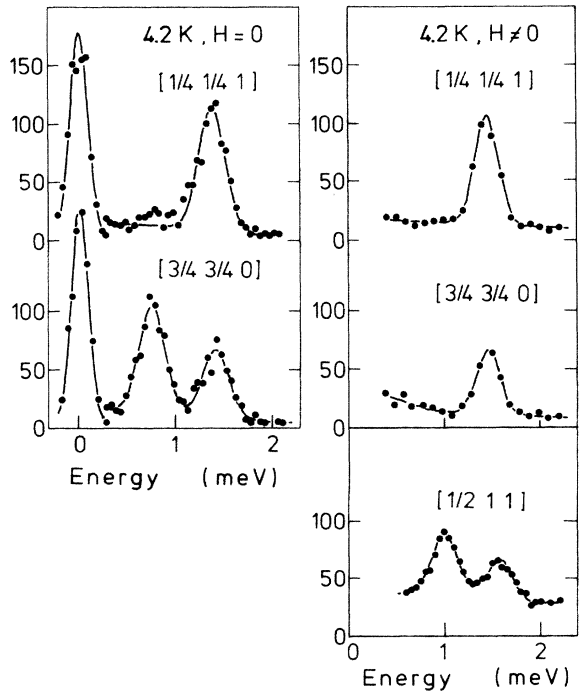

FIG. 7. INS spectra of the Γ_7 excitation in CeAs for the AF-I multidomain state ($\mathbf{H}=\mathbf{0}$) and the AF-I z domain ($\mathbf{H}\neq\mathbf{0}$).

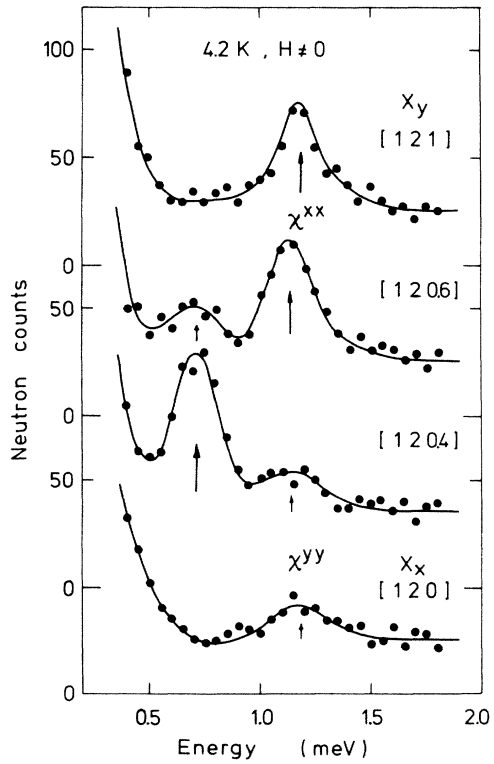

FIG. 9. INS spectra in the AF-I z domain of CeAs for wave vectors along $[10q]$. The strong peak (long arrow) and the weak peak (short arrow) indicate the xx and yy excitations, respectively.

the peak at $(00\frac{3}{2})$ is observed (Fig. 10), which supports the existence of two slightly different high-energy excitations at $(00\frac{3}{2})$. Furthermore, INS measurements in zero field at $T=2$ K (where line broadening due to relaxation effects become negligibly small) clearly show two higher-energy peaks in the multidomain state at $(00\frac{3}{2})$ (Fig. 11). Above INS experiments undoubtedly prove the multidomain single-$\mathbf{q}$ AF-I state for CeAs in zero field.

The particular magnetic excitation behavior observed in CeAs is the consequence of anisotropic bilinear exchange interactions. In fact, the model derived in Sec. II excellently describes the magnetic excitations in the ordered state as shown below. As a first step we have neglected the single-ion anisotropy due to higher-lying quartet states and the quadrupolar interactions. The two isolated Γ_7 levels then form an effective $S=\frac{1}{2}$ system with $S=\langle S^z\rangle=\pm\frac{5}{6}$ at $T=0$, and the calculation for the two-level model [Eq. (39)] applies. For the z domain the molecular-field splitting becomes $\Delta=4S^2J^{zz}(\mathbf{q}_0^z)=4S^2J_0$, and the matrix element is $M=4S^2$. For the dispersion behavior of the magnetic excitations we then get

$$\begin{aligned}\omega^{xx}(\mathbf{q})&=4S^2\{[J_0-J^{xx}(\mathbf{q})][J_0-J^{yy}(\mathbf{q}+\mathbf{q}_0^z)]\}^{1/2}\,,\\ \omega^{yy}(\mathbf{q})&=4S^2\{[J_0-J^{yy}(\mathbf{q})][J_0-J^{xx}(\mathbf{q}+\mathbf{q}_0^z)]\}^{1/2}\,.\end{aligned}\tag{50}$$

At the X_x point the xx excitation becomes $\omega^{xx}(\mathbf{q})=0$, since $J^{xx}(X_x)=J_0$ and $J^{yy}(X_x+\mathbf{q}_0^z)=J^{yy}(X_y)=J_0$, and similarly $\omega^{yy}(\mathbf{q})=0$ at the X_y point. However, at the X_z point both excitations ω^{xx} and ω^{yy} have nonzero energy, so that the observed behavior of the magnetic excitations is correctly reproduced. The quadratic dispersion at the X point is obtained by expanding the exchange coupling tensor:

$$\begin{aligned}\omega^{xx}(\mathbf{q}=(1+q,0,0))&=\omega^{xx}(\mathbf{q}=(1,q,0))\\&=16S^2\pi^2A_1A_2q^2+\cdots\,,\\ \omega^{xx}(\mathbf{q}=(1,0,q))&=16S^2\pi^2A_1^2q^2+\cdots\end{aligned}\tag{51}$$

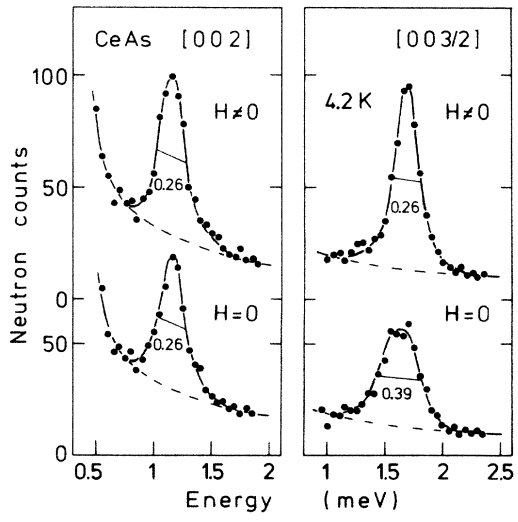

FIG. 10. INS spectra in the AF-I multidomain state ($\mathbf{H}=\mathbf{0}$) and the AF-I z domain ($\mathbf{H}\neq\mathbf{0}$) of CeAs at $T=4.2$ K.

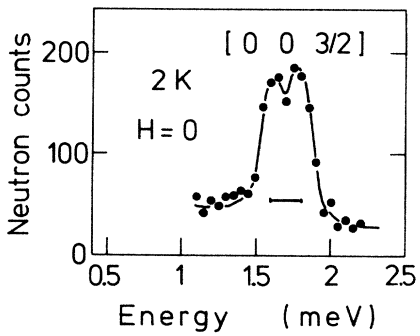

FIG. 11. INS spectrum in CeAs in the AF-I multidomain state at $T=2$ K. The resolution is indicated by the horizontal bar.

with

$$\begin{aligned}A_1&=(-\tfrac{1}{2}J_1^l+\tfrac{1}{2}J_1^t+J_2^t+J_3^l-5J_3^t\\&\quad+2J_4^l+2J_4^t+\cdots)^{1/2}\,,\\ A_2&=(-J_1^l+J_2^l+4J_3^l-2J_3^t+4J_4^l+\cdots)^{1/2}\,.\end{aligned}$$

Obviously, the dispersion minimum displays the tetragonal symmetry of the exchange tensor.

We arrive at the interesting result that any $S=\frac{1}{2}$, type-I, fcc antiferromagnet with anisotropic exchange interactions exhibits the above excitation behavior with a mode going quadratically to zero at the AF-I centers with $\mathbf{q}\neq\mathbf{q}_0$. The system once ordered with $\mathbf{q}_0^\alpha$ immediately displays a "soft mode" at the other $\mathbf{q}_0^\beta$. Any of the equivalent longitudinal $\langle 001\rangle$ waves shows a zero-energy excitation with respect to another $\langle 001\rangle$ wave. Similar to the ferromagnets these systems show the behavior that the magnetic moments are not fixed to a certain direction. The spins can turn around in a way compatible with the AF-I ordering without any restoring force leading to the zero-energy spin waves with a quadratic dispersion.

In CeAs a small single-ion anisotropy is produced by the crystal-field and the quadrupolar interactions. A detailed RPA calculation [Eq. (32)] with the full six-level scheme takes the single-ion anisotropy into account. The spin-wave dispersion curves at $T=4.2$ K as well as the crystal-field excitations in the paramagnetic state yield the best-fit values of the model parameters as listed in Table II. The off-diagonal elements of the interaction tensor are negligibly small, since no splitting of the excitations along

TABLE II. "Best-fit" values for the system parameters of CeAs.

$B_4=0.036\pm0.001$ meV
$J_0=0.392\pm0.006$ meV
$K_0=0.045\pm0.005$ meV
$J_1^l=-28\pm2\ \mu$eV, $J_1^t=16\pm4\ \mu$eV, $J_1^q\sim0$
$J_2^l=20\pm5\ \mu$eV, $J_2^t=25\pm2\ \mu$eV,
$J_3^l=0\pm2\ \mu$eV, $J_3^t=4\pm2\ \mu$eV, $J_3^{q1},J_3^{q2}\sim0$
$J_4^l=2\pm2\ \mu$eV, $J_4^t=0\pm2\ \mu$eV, $J_4^q\sim0$

[qqq] has been observed [Fig. 5(c) and Eq. (44)]. Figure 12 shows the calculated zz component of the Fourier-transformed bilinear exchange interaction tensor along the different symmetry directions. The anisotropy of the coupling is especially pronounced at the X points, where

$$J^{zz}(X_z) \gg J^{zz}(X_x) = J^{zz}(X_y)$$

is consistent with the DCNS result.

The parameter set obtained from the excitation measurements using the model derived in Sec. II gives a consistent description of the static and dynamic magnetic properties of CeAs. The spin-wave dispersion curves at $T=4.2$ K and the crystal-field excitations in the paramagnetic state are excellently reproduced in detail (Fig. 5). The temperature dependence of the doublet splitting is perfectly predicted as exemplified for the excitation at $(\frac{1}{2}\frac{1}{2}\frac{1}{2})$ (Fig. 13). The calculated ordering temperature T_N and the calculated zero-field moment μ_0

$$T_N = 8.7 \pm 0.3 \text{ K},$$

$$\mu_0 = (0.94 \pm 0.01)\mu_B$$

are very close to the actual values listed in Table I. Inserting the exchange parameters into Eq. (47) for the anisotropy of the correlation lengths in the critical temperature region above T_N yields

$$\kappa_{\parallel}/\kappa_{\perp} = 0.8 \pm 0.2,$$

which is in good agreement with the lenslike intensity distribution observed in the DCNS experiments (Sec. IV). Finally the parameter set is consistent with the AF-I single-**q** ordering of CeAs: the large quadrupole interaction dominates the [111] easy direction predicted by the crystal field and slightly favors a [001] alignment of the spins with an extremely small anisotropy gap of ~ 0.03 meV. Obviously CeAs is an almost ideal model $S=\frac{1}{2}$ antiferromagnet.

B. CeSb, AF-IA single-q structure

Below $T_N = 16.4$ K, CeSb exhibits various magnetic phases with different stackings of ferromagnetic (001) planes with up or down spins and paramagnetic planes.[2,3] The magnetic ordering is accompanied by a tetragonal lattice distortion[4] directly indicating collinear single-**q** spin configurations. In an external magnetic field $|\mathbf{H}||[001]| > 38$ kOe and for temperatures $T < 10$ K in CeSb ferromagnetic ordering is obtained.[37] In this state the crystal is a single domain with $\boldsymbol{\mu}||[001]$ and the interpretation of INS experiments is straightforward. Thus the magnetic excitations of CeSb were first measured at $T=4.2$ K and $|\mathbf{H}||[001]| = 42$ kOe. For geometrical reasons (**H** perpendicular to the scattering plane) only wave vectors along the symmetry directions [$q00$] and [$qq0$] were accessible. The measurements show a magnetic excitation at ~ 4 meV with a dispersion considerably different along the above symmetry directions [Fig. 14(a)]. The excitation energy is 4.2 meV at the X_z point but 3.3 meV at the X_x point, which is a direct consequence of anisotropic magnetic interactions. However, as expected for the ferromagnetic state [Eq. (38)], the excitation does not split into different modes although the couplings are strongly anisotropic.

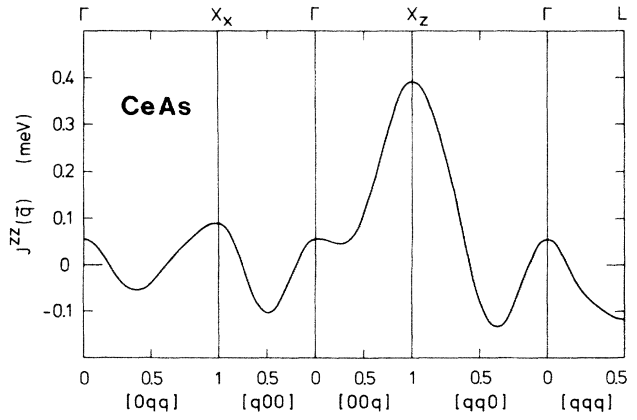

FIG. 12. Bilinear exchange interaction $J^{zz}(\mathbf{q})$ resulting for CeAs. $J^{xx}(\mathbf{q})$ and $J^{yy}(\mathbf{q})$ look the same with the appropriate permutation of the symmetry directions.

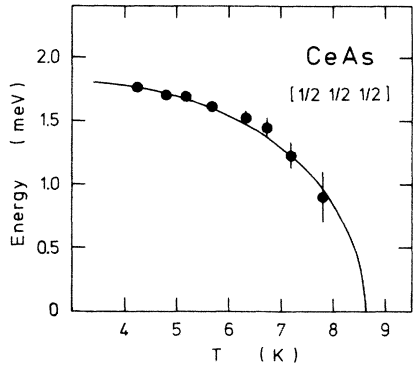

FIG. 13. Experimentally observed and calculated temperature behavior of the magnetic excitation in CeAs at the L point.

Without external field the magnetic phases of CeSb above $T \sim 9$ K correspond to complicated antiferromagnetic structures with periods up to 13 unit cells, so that the analysis of the magnetic excitations becomes rather difficult. Below $T \sim 9$ K, however, the AF-IA structure is realized and the corresponding RPA formalism was developed in Sec. II. In the AF-IA state at $T=4.2$ K and $\mathbf{H}=0$, INS experiments were performed for wave vectors along [$00q$], [$qq0$], and [qqq]. As in the ferromagnetic state a magnetic excitation at ~ 4 meV with a moderate dispersion is observed. At the AF-I centers or the X points two excitation peaks at 3.2 and 4.2 meV appear (Fig. 15), indicating an apparent splitting of the spin-wave excitation into two modes similar to CeAs. The intensity behavior of the two peaks, however, is different from that of the AF-I magnets. In contrast to CeAs, in CeSb both excitations are observed at (110) as well as at (001). The only effect is a change in their intensities towards a stronger lower-energy excitation by going from (001) to (112) and (110) (Fig. 15).

In order to identify the contributions of the different domains a single-domain AF-IA state of CeSb was created by cooling the sample in an external magnetic field

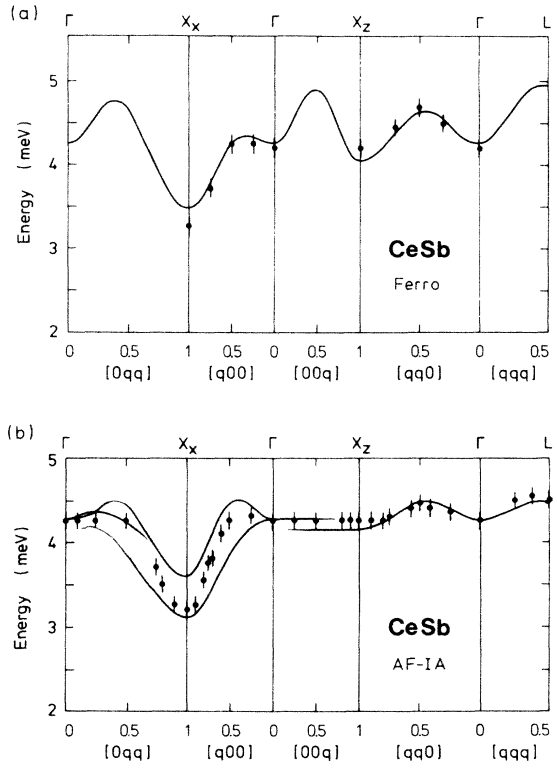

FIG. 14. Dispersion curves of the magnetic excitations in CeSb at $T=4.2$ K: (a) in the ferromagnetic state with $|\mathbf{H}||[001]|=42$ kOe; (b) in the AF-IA z domain with $\mathbf{H}=\mathbf{0}$. The solid lines are the result of the RPA calculation described in the text. The thickness of the lines roughly indicates the intensity of the corresponding excitation.

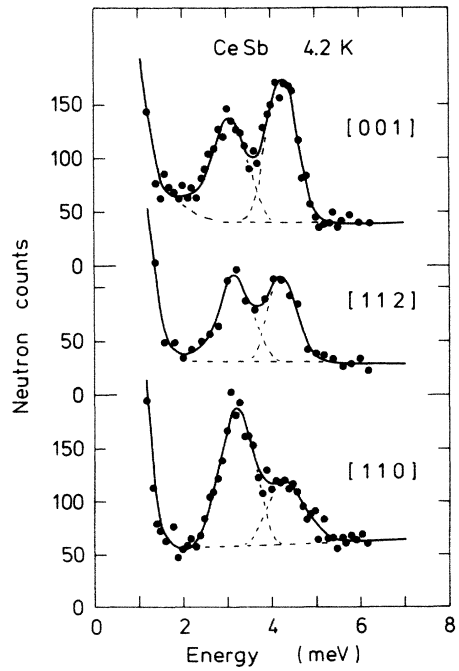

FIG. 15. INS spectra in the multidomain AF-IA state ($T=4.2$ K, $\mathbf{H}=\mathbf{0}$) of CeSb observed at different X points.

$|\mathbf{H}||[001]|>20$ kOe through the ordering temperature and then slowly reducing the field to zero. Now the magnetic excitations of the AF-IA z domain along $[q00]$ and $[qq0]$ may be measured. It turned out that the two excitation peaks observed in the multidomain state at the X points (Fig. 15) have to be assigned to different domains. The dispersion curves resulting for the AF-IA z domain of CeSb are shown in Fig. 14(b) in the full nuclear fcc Brillouin zone with respect to the tetragonal symmetry of the single-$\mathbf{q}$ configuration. The single domain essentially has only one excitation peak which has transverse character. The xx and yy excitations are almost or fully degenerate. A comparison of the excitation spectra at (020) and (120) for the ferromagnetic and AF-IA z-domain state, however, reveals undoubtedly a broadening of the neutron peak at the X_x point in the AF-IA phase (Fig. 16). Thus, the excitation at the X_x point may be slightly split into two modes with xx or yy polarization [as indicated by the theoretical line in Fig. 14(b)]. In Fig. 14(b) for each $\mathbf{q}$ a single experimental point is given since the anticipated splitting into different modes could not be resolved in the present measurements.

The magnetic excitations in CeSb observed in the multidomain AF-AI state are understood in terms of a superposition of the appropriate spectra [Fig. 14(b)] of the three equivalent x,y,z domains. The intensity behavior at the X points (Fig. 15) differs from CeAs, since in CeSb the xx and yy excitations are almost degenerate at X_x and X_y, whereas in the AF-I magnet CeAs they are strongly split at these points.

As in the AF-I magnet CeAs [Fig. 5(c)] the magnetic excitations in the ferromagnetic and the AF-IA z-domain state of CeSb (Fig. 14) have a pronounced energy minimum at the X_x and X_y points. This immediately indicates that similar to CeAs the magnetic interactions in CeSb have a maximum at the AF-I centers which is con-

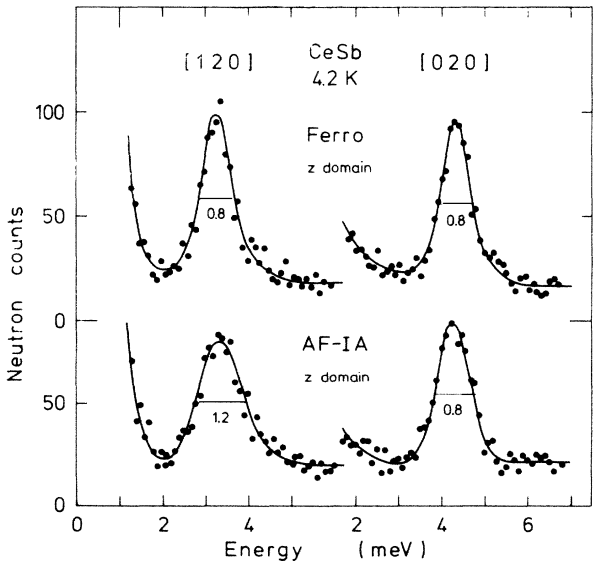

FIG. 16. INS spectra at the X_x and the Γ point of CeSb in the ferromagnetic state ($|\mathbf{H}||[001]|=42$ kOe) and for the AF-IA z domain.

sistent with the AF-I fluctuations observed in the paramagnetic state of CeSb (Refs. 16 and 17) (Fig. 4).

At $T=4.2$ K the magnetic moment of CeSb is saturated and nearly has the free-ion value (Table I). Then the ground state is an almost pure $|\frac{5}{2}\rangle$ state and the only possible magnetic excitation is the $|\frac{5}{2}\rangle \rightarrow |\frac{3}{2}\rangle$ transition which has transverse character. Thus, CeSb at $T=4.2$ K may be considered as a two-level system, and the magnetic excitations follow Eq. (38) for the ferromagnetic state and Eq. (40) for the AF-IA state. The transition matrix element is $M=5$ and the splitting of the single-ion levels is given by the parameter Δ_F or $\Delta_{\text{AF-IA}}$ for the ferromagnetic or AF-IA state, respectively. A "least-squares fit" of the above equations to the experimental data for the magnetic excitations in the F and AF-IA state, taking into account the temperature dependence of the critical AF-I fluctuations and their anisotropy $\kappa_{\parallel}/\kappa_{\perp}$, yields the system parameters displayed in Table III and Fig. 17. As in CeAs the exchange interactions were assumed to be diagonal, since the transition along $[qqq]$ does not split into different modes. The parameter set excellently describes the magnetic excitations in the ferromagnetic and antiferromagnetic states (Fig. 14) as well as the quasistatic fluctuations in the paramagnetic state with a virtual divergence at $T\sim 14$ K (Ref. 16) and anisotropic correlation lengths $\kappa_{\parallel}/\kappa_{\perp}=1.3\pm 0.5$.

There is a remarkable similarity of the bilinear exchange interactions $J^{zz}(\mathbf{q})$ found in CeSb (Fig. 17) and those of CeAs (Fig. 12) although the static and dynamic behavior of the two compounds is considerably different. In CeSb as in CeAs, $J^{zz}(\mathbf{q})$ shows a well-defined maximum at the X_z point. Obviously the bilinear exchange interactions in CeSb favor an AF-I structure, although a long-range-ordered state of this type is not realized. Thus, all the magnetic phases of CeSb are not forced by the bilinear exchange coupling, but are the result of the lattice distortion or higher-order magnetic interactions. Indeed this has been recently demonstrated for the diluted system $Ce_{1-x}(La,Y)_xSb$.[17] The higher-order interactions are also responsible for the large single-ion anisotropy of CeSb with [001] as the easy axis instead of [111] predicted by the crystal field.

The magnetic excitation spectra observed in CeSb indicate that the single-ion levels of the Ce^{3+} ions in the ordered state are almost pure Zeeman levels. Obviously, the molecular fields dominate over the crystal field. The molecular-field parameter J_0 for the F or AF-IA state is given by the two-ion exchange parameters obtained from the dispersion behavior of the magnetic excitations (Table III). Then to obtain the observed Zeeman levels with an energy splitting Δ_F or $\Delta_{\text{AF-IA}}$ of the two lowest-lying levels the crystal-field parameter B_4 has to be negligibly small, and for the quadrupole interactions we get $K_0\sim 20$ μeV which is the size needed to correctly predict the first-order transition to the magnetically ordered state at T_N as well as the strong [001] single-ion anisotropy of CeSb. The apparent disappearance of the crystal field in the ordered state of CeSb is a very unusual phenomenon. In the paramagnetic state INS experiments showed a crystal-field transition from which $B_4=8.9$ μeV was deduced.[38] Thus, in contrast to other rare-earth systems, in CeSb the strength of the fourth-order crystal-field terms is not conserved in the phase transition at T_N. Undoubtedly, B_4 is drastically reduced in the ordered state. The tetragonal lattice distortion alone is not able to take into account the reduction of B_4 mentioned above. Rather, it seems that the disappearance of the crystal field has to be understood in conjunction with the anomalous magnetic interactions in CeSb.

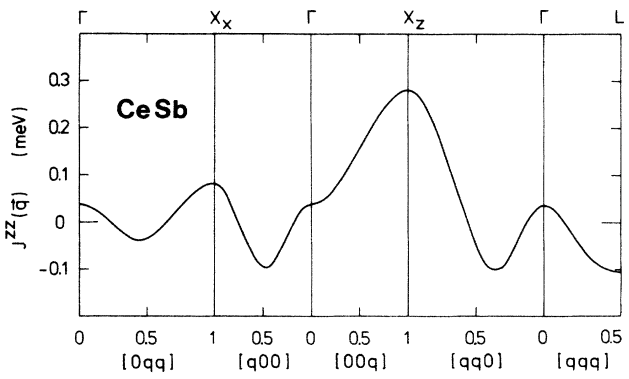

FIG. 17. Bilinear exchange coupling $J^{zz}(\mathbf{q})$ resulting for CeSb.

The experimental data available for CeSb quite reliably define the bilinear exchange interactions $J^{\alpha\beta}(\mathbf{q})$ and give an estimate for B_4 and K_0. The individual two-ion quadrupole or higher-order interactions, however, are still unknown. High-resolution INS experiments and a generalization of the RPA theory to include higher-order interactions would give more insight into the anomalous coupling mechanism in CeSb.

CeBi exhibits a nearly identical magnetic excitation spectrum[19] as observed for CeSb, and similar arguments concerning the magnetic interactions will hold. CeBi shows in addition to the low-temperature AF-IA phase a high-temperature AF-I state which directly confirms the bilinear magnetic interactions of AF-I type already found for CeSb.

TABLE III. "Best-fit" values for the system parameters of CeSb.

$M=5$ ($\lvert\frac{5}{2}\rangle \rightarrow \lvert\frac{3}{2}\rangle$)
$\Delta_F=4.5\pm 0.1$ meV
$\Delta_{\text{AF-IA}}=4.13\pm 0.1$ meV
$J_1^l=-21\pm 2$ μeV, $J_1^t=14\pm 5$ μeV, $J_1^q\sim 0$
$J_2^l=13\pm 9$ μeV, $J_2^t=22\pm 8$ μeV,
$J_3^l=-2\pm 3$ μeV, $J_3^t=3\pm 2$ μeV, $J_3^{q1}, J_3^{q2}\sim 0$
$J_4^l=-1\pm 2$ μeV, $J_4^t=3\pm 4$ μeV, $J_4^q\sim 0$

C. USb, AF-I triple-q structure

USb orders below $T_N\sim 220$ K in the AF-I structure. Pressure experiments[1] indicate a noncollinear triple-$\mathbf{q}$ configuration with the moments along [111]. In contrast to the cerium systems INS experiments in the uranium

monopnictides usually show only a diffuse response[21,22] and fail to find any discrete crystal-field levels which could give evidence for localized $5f$ states. An exception is USb, for which Lander *et al.*[20] found a well-defined spin-wave mode with an anisotropy gap of ~ 6.4 meV at the X points and a broad excitonic magnetic level at ~ 26 meV. However, the spin-wave excitation showed an unexpected longitudinal character. Jensen and Bak[23] found an explanation for the longitudinal character of the excitation in terms of spin waves in a triple-**q** structure.

The magnetic excitation behavior of USb, which is very similar to that of CeAs, has been reinvestigated in detail. In the ordered state at $T=10$ K, INS experiments for wave vectors along the cubic symmetry directions $[00q]$, $[qq0]$, and $[qqq]$ were performed. The observed spectra always have a considerable contribution of phonon scattering. However, the dispersion curves and the intensities of the phonons are well known, which essentially simplifies the identification of the magnetic scattering. In Fig. 18 the resulting energies of the observed magnetic excitations are summarized. In contrast to Lander *et al.*,[20] the excitation at ~ 26 meV was found to be a well-resolved spin-wave excitation.

Similar to CeAs the spin-wave excitation in USb is split into two modes at the X points. Near (003) only the energetically higher mode is observed, whereas near (221) the same mode has half the intensity, but in addition the lower-energy mode appears (Fig. 19). This behavior might mislead one to assign a longitudinal character to the lower excitation mode,[20] but, as in CeAs, it has to be understood in terms of transverse spin waves in an AF-I magnet with anisotropic interactions.

For the AF-I triple-**q** structure the magnetic excitations have been calculated in Sec. II. Since USb at $T=10$ K has nearly the full moment, the transverse $|\frac{9}{2}\rangle \rightarrow |\frac{7}{2}\rangle$ transition dominates (here transverse means with respect to the spin direction or [111]). Thus, as a first approximation Eq. (43) with only the transition between the two lowest-lying levels may be considered. At least two of the resulting excitations $\omega^{xx}(\mathbf{q})$, $\omega^{yy}(\mathbf{q})$, and $\omega^{zz}(\mathbf{q})$ are always degenerate by the symmetry of the anisotropic exchange

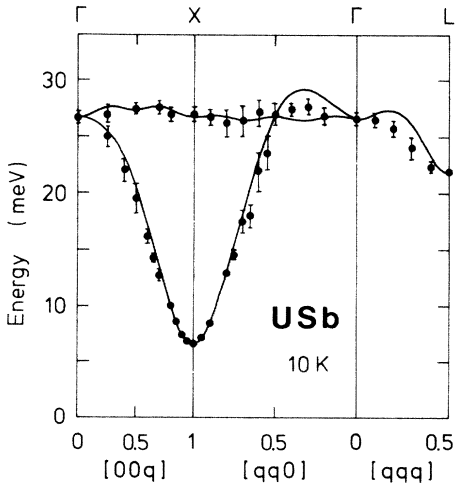

FIG. 18. Experimentally observed and calculated dispersion curves for USb in the AF-I triple-**q** ordered state at $T=10$ K.

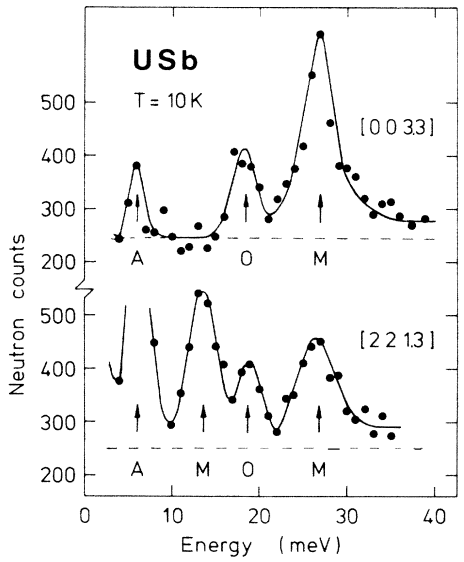

FIG. 19. INS spectra near the X points in USb: The arrows indicate the magnetic excitations (M), the optical (O), and the acoustical (A) phonons, respectively.

interactions. For the X_z point we get $\omega^{xx}(X_z)=\omega^{yy}(X_z) \neq \omega^{zz}(X_z)$. By the polarization factor near (003) only the degenerate xx and yy excitations are observed at ~ 26 meV. However, in the vicinity of (221) the xx and yy excitations have half the intensity, and the zz excitation appears with a much lower energy (see Fig. 19).

Using a numerical full ten-level calculation [Eq. (34)] of the magnetic excitations in USb, a reasonable description of the neutron data at $T=10$ K is obtained (Fig. 18). Taking into account the actual ordering temperature T_N and the anisotropy of the correlation lengths $\kappa_{\parallel}/\kappa_{\perp}$ above T_N, we arrive at the "best-fit" values for the system parameters listed in Table IV. The crystal-field parameters B_4 and B_6 are in the notation of Ref. 39: $B_4=Wx/60$ and $B_6=W(1-|x|)/2520$. For the triple-**q** structure with the magnetic moments along [111] the quadrupole moments $\langle O_2^0 \rangle$ and $\langle O_2^2 \rangle$ vanish, and K_0 becomes irrelevant. Furthermore, similar to CeAs and CeSb diagonal exchange interaction tensors were assumed, since there is no observable splitting of the spin-wave excitation along $[qqq]$. The resulting zz component of the Fourier-transformed exchange interaction $J^{zz}(\mathbf{q})$ is shown in Fig. 20. With the parameters in Table IV the calculated ordering temperature, the ordered moment, and the anisotropy of the inverse correlation lengths become

$$T_N = 240 \pm 20 \text{ K} ,$$

$$\mu_0 = (2.73 \pm 0.05)\mu_B ,$$

$$\kappa_{\parallel}/\kappa_{\perp} = 5.2 \pm 2.0 ,$$

which are in good agreement with the actual values (Table I).

Jensen and Bak[23] calculated the excitation spectrum of USb by ordinary spin-wave theory in the triple-**q** structure with pseudodipolar exchange interactions. The large

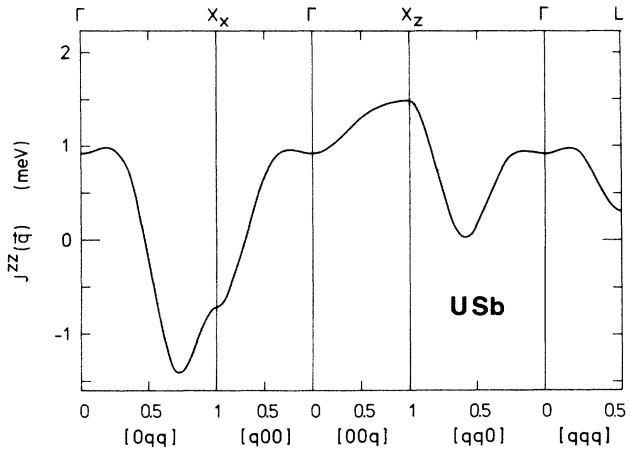

FIG. 20. Bilinear exchange interaction $J^{zz}(\mathbf{q})$ resulting for USb.

off-diagonal elements of their interaction tensors should produce a splitting of the spin wave into different modes along $[qqq]$ which is not experimentally observed. Furthermore, based on the excitation spectrum they calculate an ordering temperature which is far above the actual value.

In addition to the size of the exchange couplings our RPA treatment of the magnetic excitations provides information on the crystal field. The set of crystal-field parameters given in Table IV predicts for the U^{3+} ions in USb the quartet $\Gamma_8^{(1)}$ as the ground state and the doublet Γ_6 at 100 meV and the quartet $\Gamma_8^{(2)}$ at 104 meV as the excited states. The crystal field strongly favors an alignment of the spins along $\langle 111 \rangle$ corresponding to the triple-$\mathbf{q}$ structure. The large single-ion anisotropy due to the crystal field is directly responsible for the energy gap of ~ 6 meV at the X points.

The crystal-field concept with localized $5f$ electrons successfully applies to USb and yields a consistent description of the magnetic excitations at $T=10$ K as well as static properties such as T_N, the triple-$\mathbf{q}$ configuration and the ordered moment. Compared to the CeX compounds, however, for USb a considerably larger crystal field is expected. It seems that the $5f$ electrons in USb are rather localized as already found from photoemission experiments.[40]

TABLE IV. "Best-fit" values for the system parameters of USb.

$x=0.82\pm0.02$, $W=1.9\pm0.3$ meV,
($B_4=25.6$ μeV, $B_6=0.14$ μeV)
$J_0=1.48\pm0.05$ meV
$J_1^l=35\pm5$ μeV, $J_1^l=383\pm50$ μeV, $J_1^q\sim0$
$J_2^l=110\pm8$ μeV, $J_2^l=-65\pm6$ μeV,
$J_3^l=-72\pm4$ μeV, $J_3^l=-35\pm3$ μeV, $J_3^{q1}, J_3^{q2}\sim0$
$J_4^l=38\pm3$ μeV, $J_4^l=-7\pm5$ μeV, $J_4^q\sim0$

VI. SUMMARY

In this paper we have given a detailed theoretical and experimental investigation on the anomalous anisotropic magnetic interactions present in the cerium and uranium monopnictides and their effects on the spin dynamics in the paramagnetic as well as in the AF-I or related magnetically ordered state. For CeAs, CeSb, and USb inelastic and diffuse critical neutron scattering experiments have been performed. Undoubtedly the chief benefit of such experiments results from the magnetic excitations which contain a lot of information on the anisotropic interactions present in these systems, thus providing detailed answers to several key problems. Once the magnetic excitation spectrum is measured with sufficient accuracy, properly disentangled from the domain problem, and analyzed by an appropriate Hamiltonian, the resulting model parameters can reliably predict the magnetic behavior of the system. We particularly emphasize the complete consistency that is obtained for CeAs, CeSb, and USb in describing the anisotropy of both the spin waves which are transverse excitations, and the critical scattering which corresponds to longitudinal fluctuations, as well as static properties such as the magnetic structure, the ordering temperature, and the ordered moment.

Apart from a scaling factor a remarkable similarity of the bilinear exchange interactions was found for CeAs, CeSb, and USb, although these systems exhibit a completely different static and dynamic behavior. This directly demonstrates the drastical influence of the magnetic structure on the actually observed excitation spectrum. Furthermore, it is interesting to note that for all compounds negligibly small off-diagonal exchange couplings were obtained. The anisotropic interactions derived in this paper must be considered as phenomenological parameters, but they may provide a useful quantitative basis for theoretical investigations on the origin of the large magnetic anisotropy or on the nature of the phase transitions in the CeX and UX compounds.

In the paper we showed that bilinear exchange alone does not explain all the magnetic phenomena observed in the cerium and uranium monopnictides. Higher-order magnetic interactions are present in these systems as was undoubtedly found from the study of CeSb, where bilinear exchange is not the dominant mechanism driving the system through the various phase transitions. Indeed the importance of higher-order interactions has recently been emphasized in a detailed theoretical study explaining the anomalous magnetic properties of the cerium monopnictides in terms of the anisotropic p-f mixing mechanism, which requires higher-order couplings to express the effective two-ion f-f interactions in terms of spin operators.[30]

ACKNOWLEDGMENTS

We are indebted to O. Vogt and K. Mattenberger for their valuable efforts in growing large single crystals, to J. K. Kjems for fruitful discussions and collaboration in part of the experimental work, and to B. R. Cooper for stimulating discussions. Financial support by the Swiss National Science Foundation is gratefully acknowledged.

APPENDIX: ANISOTROPIC BILINEAR INTERACTIONS IN THE fcc LATTICE

The most general symmetrically allowed coupling tensors for the four first-neighbor shells in the fcc lattice are the following.

For nearest neighbors,

$$J_{0j}=\begin{bmatrix} J_1^l & \pm J_1^a & 0 \\ \pm J_1^a & J_1^l & 0 \\ 0 & 0 & J_1^t \end{bmatrix} \text{ for } \mathbf{R}_j=\begin{cases} a(\frac{1}{2},\pm\frac{1}{2},0) \\ a(-\frac{1}{2},\mp\frac{1}{2},0)\ , \end{cases}$$

$$J_{0j}=\begin{bmatrix} J_1^l & 0 & \pm J_1^a \\ 0 & J_1^t & 0 \\ \pm J_1^a & 0 & J_1^l \end{bmatrix} \text{ for } \mathbf{R}_j=\begin{cases} a(\frac{1}{2},0,\pm\frac{1}{2}) \\ a(-\frac{1}{2},0,\mp\frac{1}{2})\ , \end{cases}$$

$$J_{0j}=\begin{bmatrix} J_1^t & 0 & 0 \\ 0 & J_1^l & \pm J_1^a \\ 0 & \pm J_1^a & J_1^l \end{bmatrix} \text{ for } \mathbf{R}_j=\begin{cases} a(0,\frac{1}{2},\pm\frac{1}{2}) \\ a(0,-\frac{1}{2},\mp\frac{1}{2})\ . \end{cases}$$

For second-nearest neighbors,

$$J_{0j}=\begin{bmatrix} J_2^l & 0 & 0 \\ 0 & J_2^t & 0 \\ 0 & 0 & J_2^t \end{bmatrix} \text{ for } \mathbf{R}_j=a(\pm1,0,0)\ ,$$

$$J_{0j}=\begin{bmatrix} J_2^t & 0 & 0 \\ 0 & J_2^l & 0 \\ 0 & 0 & J_2^t \end{bmatrix} \text{ for } \mathbf{R}_j=a(0,\pm1,0)\ ,$$

$$J_{0j}=\begin{bmatrix} J_2^t & 0 & 0 \\ 0 & J_2^t & 0 \\ 0 & 0 & J_2^l \end{bmatrix} \text{ for } \mathbf{R}_j=a(0,0,\pm1)\ .$$

For third-nearest neighbors,

$$J_{0j}=\begin{bmatrix} J_3^t & J_3^{a1} & J_3^{a2} \\ J_3^{a1} & J_3^t & J_3^{a2} \\ J_3^{a2} & J_3^{a2} & J_3^l \end{bmatrix} \text{ for } \mathbf{R}_j=a(\pm\tfrac{1}{2},\pm\tfrac{1}{2},\pm1)\ ,$$

$$J_{0j}=\begin{bmatrix} J_3^t & -J_3^{a1} & J_3^{a2} \\ -J_3^{a1} & J_3^t & -J_3^{a2} \\ J_3^{a2} & -J_3^{a2} & J_3^l \end{bmatrix} \text{ for } \mathbf{R}_j=a(\pm\tfrac{1}{2},\mp\tfrac{1}{2},\pm1)\ ,$$

$$J_{0j}=\begin{bmatrix} J_3^t & -J_3^{a1} & -J_3^{a2} \\ -J_3^{a1} & J_3^t & J_3^{a2} \\ -J_3^{a2} & J_3^{a2} & J_3^l \end{bmatrix} \text{ for } \mathbf{R}_j=a(\mp\tfrac{1}{2},\pm\tfrac{1}{2},\pm1)\ ,$$

$$J_{0j}=\begin{bmatrix} J_3^t & J_3^{a1} & -J_3^{a2} \\ J_3^{a1} & J_3^t & -J_3^{a2} \\ -J_3^{a2} & -J_3^{a2} & J_3^l \end{bmatrix} \text{ for } \mathbf{R}_j=a(\mp\tfrac{1}{2},\mp\tfrac{1}{2},\pm1)\ ,$$

$$J_{0j}=\begin{bmatrix} J_3^t & J_3^{a2} & J_3^{a1} \\ J_3^{a2} & J_3^l & J_3^{a2} \\ J_3^{a1} & J_3^{a2} & J_3^t \end{bmatrix} \text{ for } \mathbf{R}_j=a(\pm\tfrac{1}{2},\pm1,\pm\tfrac{1}{2})\ ,$$

$$J_{0j}=\begin{bmatrix} J_3^t & J_3^{a2} & -J_3^{a1} \\ J_3^{a2} & J_3^l & -J_3^{a2} \\ -J_3^{a1} & -J_3^{a2} & J_3^t \end{bmatrix} \text{ for } \mathbf{R}_j=a(\pm\tfrac{1}{2},\pm1,\mp\tfrac{1}{2})\ ,$$

$$J_{0j}=\begin{bmatrix} J_3^t & -J_3^{a2} & -J_3^{a1} \\ -J_3^{a2} & J_3^l & J_3^{a2} \\ -J_3^{a1} & J_3^{a2} & J_3^t \end{bmatrix} \text{ for } \mathbf{R}_j=a(\mp\tfrac{1}{2},\pm1,\pm\tfrac{1}{2})\ ,$$

$$J_{0j}=\begin{bmatrix} J_3^t & -J_3^{a2} & J_3^{a1} \\ -J_3^{a2} & J_3^l & -J_3^{a2} \\ J_3^{a1} & -J_3^{a2} & J_3^t \end{bmatrix} \text{ for } \mathbf{R}_j=a(\mp\tfrac{1}{2},\pm1,\mp\tfrac{1}{2})\ ,$$

$$J_{0j}=\begin{bmatrix} J_3^l & J_3^{a2} & J_3^{a2} \\ J_3^{a2} & J_3^t & J_3^{a1} \\ J_3^{a2} & J_3^{a1} & J_3^t \end{bmatrix} \text{ for } \mathbf{R}_j=a(\pm1,\pm\tfrac{1}{2},\pm\tfrac{1}{2})\ ,$$

$$J_{0j}=\begin{bmatrix} J_3^l & J_3^{a2} & -J_3^{a2} \\ J_3^{a2} & J_3^t & -J_3^{a1} \\ -J_3^{a2} & -J_3^{a1} & J_3^t \end{bmatrix} \text{ for } \mathbf{R}_j=a(\pm1,\pm\tfrac{1}{2},\mp\tfrac{1}{2})\ ,$$

$$J_{0j}=\begin{bmatrix} J_3^l & -J_3^{a2} & J_3^{a2} \\ -J_3^{a2} & J_3^t & -J_3^{a1} \\ J_3^{a2} & -J_3^{a1} & J_3^t \end{bmatrix} \text{ for } \mathbf{R}_j=a(\pm1,\mp\tfrac{1}{2},\pm\tfrac{1}{2})\ ,$$

$$J_{0j}=\begin{bmatrix} J_3^l & -J_3^{a2} & -J_3^{a2} \\ -J_3^{a2} & J_3^t & J_3^{a1} \\ -J_3^{a2} & J_3^{a1} & J_3^t \end{bmatrix} \text{ for } \mathbf{R}_j=a(\pm1,\mp\tfrac{1}{2},\mp\tfrac{1}{2})\ .$$

For fourth-nearest neighbors,

$$J_{0j}=\begin{bmatrix} J_4^l & \pm J_4^a & 0 \\ \pm J_4^a & J_4^l & 0 \\ 0 & 0 & J_4^t \end{bmatrix} \text{ for } \mathbf{R}_j=\begin{cases} a(1,\pm1,0) \\ a(-1,\mp1,0)\ , \end{cases}$$

$$J_{0j}=\begin{bmatrix} J_4^l & 0 & \pm J_4^a \\ 0 & J_4^t & 0 \\ \pm J_4^a & 0 & J_4^l \end{bmatrix} \text{ for } \mathbf{R}_j=\begin{cases} a(1,0,\pm1) \\ a(-1,0,\mp1)\ , \end{cases}$$

$$J_{0j}=\begin{bmatrix} J_4^t & 0 & 0 \\ 0 & J_4^l & \pm J_4^a \\ 0 & \pm J_4^a & J_4^l \end{bmatrix} \text{ for } \mathbf{R}_j=\begin{cases} a(0,1,\pm1) \\ a(0,-1,\mp1)\ . \end{cases}$$

The Fourier-transformed interaction tensor at $\mathbf{q}=(2\pi/a)(x,y,z)$ becomes

$$J^{\alpha\beta}(\mathbf{q})=\sum_j J_{0j}^{\alpha\beta}e^{i\mathbf{q}\cdot\mathbf{R}_j}\ ,$$

with the diagonal element

$$
\begin{aligned}
J^{zz}(\mathbf{q}) = {} & 2J_1^t\{\cos[\pi(x+y)]+\cos[\pi(x-y)]\} \\
& +2J_1^l\{\cos[\pi(x+z)]+\cos[\pi(x-z)]+\cos[\pi(y+z)]+\cos[\pi(y-z)]\} \\
& +2J_2^t[\cos(2\pi x)+\cos(2\pi y)]+2J_2^l[\cos(2\pi z)] \\
& +2J_3^l\{\cos[\pi(x+y+2z)]+\cos[\pi(x+y-2z)]+\cos[\pi(x-y+2z)]+\cos[\pi(x-y-2z)]\} \\
& +2J_3^t\{\cos[\pi(x+2y+z)]+\cos[\pi(x+2y-z)]+\cos[\pi(x-2y+z)]+\cos[\pi(x-2y-z)] \\
& \quad +\cos[\pi(2x+y+z)]+\cos[\pi(2x+y-z)]+\cos[\pi(2x-y+z)]+\cos[\pi(2x-y-z)]\} \\
& +2J_4^t\{\cos[2\pi(x+y)]+\cos[2\pi(x-y)]\}+2J_4^l\{\cos[2\pi(x+z)]+\cos[2\pi(x-z)] \\
& \quad +\cos[2\pi(y+z)]+\cos[2\pi(y-z)]\}
\end{aligned}
$$

and the off-diagonal elements

$$
\begin{aligned}
J^{xy}(\mathbf{q}) = J^{yx}(\mathbf{q}) = {} & 2J_1^a\{\cos[\pi(x+y)]-\cos[\pi(x-y)]\} \\
& +2J_3^{a\,1}\{\cos[\pi(x+y+2z)]+\cos[\pi(x+y-2z)]-\cos[\pi(x-y+2z)]-\cos[\pi(x-y-2z)]\} \\
& +2J_3^{a\,2}\{\cos[\pi(x+2y+z)]+\cos[\pi(x+2y-z)]-\cos[\pi(x-2y+z)]-\cos[\pi(x-2y-z)] \\
& \quad +\cos[\pi(2x+y+z)]+\cos[\pi(2x+y-z)]-\cos[\pi(2x-y+z)]-\cos[\pi(2x-y-z)]\} \\
& +2J_4^a\{\cos[2\pi(x+y)]-\cos[2\pi(x-y)]\}
\end{aligned}
$$

and $J^{xx}(\mathbf{q})$, $J^{yy}(\mathbf{q})$, $J^{xz}(\mathbf{q})$, $J^{yz}(\mathbf{q})$ with the appropriate cyclic permutation of x,y,z.

Along the cubic symmetry directions we obtain for $\mathbf{q}=(2\pi/a)(0,0,q)$,

$$
\begin{aligned}
J^{zz}(\mathbf{q}) = {} & 4(J_1^t+J_2^t+J_4^t)+8(J_1^l+2J_3^t)\cos(\pi q) \\
& +2(J_2^l+4J_3^l+4J_4^l)\cos(2\pi q)\ , \\
J^{xy}(\mathbf{q}) = {} & 0\ ,
\end{aligned}
$$

for $\mathbf{q}=(2\pi/a)(q,0,0)$ and $\mathbf{q}=(2\pi/a)(0,q,0)$,

$$
\begin{aligned}
J^{zz}(\mathbf{q}) = {} & 2(2J_1^l+J_2^l+J_2^t+2J_4^l) \\
& +4(J_1^l+J_1^t+2J_3^l+2J_3^t)\cos(\pi q) \\
& +2(J_2^t+4J_3^t+2J_4^l+2J_4^t)\cos(2\pi q)\ , \\
J^{xy}(\mathbf{q}) = {} & 0\ ,
\end{aligned}
$$

for $\mathbf{q}=(2\pi/a)(q,0,1)$ and $\mathbf{q}=(2\pi/a)(0,q,1)$,

$$
\begin{aligned}
J^{zz}(\mathbf{q}) = {} & 2(-2J_1^l+J_2^l+J_2^t+2J_4^l) \\
& +4(-J_1^l+J_1^t+2J_3^l-2J_3^t)\cos(\pi q) \\
& +2(J_2^t-4J_3^t+2J_4^l+2J_4^t)\cos(2\pi q)\ , \\
J^{xy}(\mathbf{q}) = {} & 0\ ,
\end{aligned}
$$

for $\mathbf{q}=(2\pi/a)(0,q,\pm q)$ and $\mathbf{q}=(2\pi/a)(q,0,\pm q)$,

$$
\begin{aligned}
J^{zz}(\mathbf{q}) = {} & 2(J_1^l+J_2^t+2J_3^t+J_4^l) \\
& +4(J_1^l+J_1^t+J_3^l+J_3^t)\cos(\pi q) \\
& +2(J_1^l+J_2^l+J_2^t+2J_3^t+2J_4^l+2J_4^t)\cos(2\pi q) \\
& +4(J_3^l+J_3^t)\cos(3\pi q)+2J_4^l\cos(4\pi q)\ , \\
J^{xy}(\mathbf{q}) = {} & 0\ ,
\end{aligned}
$$

for $\mathbf{q}=(2\pi/a)(q,\pm q,0)$,

$$
\begin{aligned}
J^{zz}(\mathbf{q}) = {} & 2(J_1^t+J_2^l+2J_3^l+J_4^t)+8(J_1^l+J_3^t)\cos(\pi q) \\
& +2(J_1^t+2J_2^t+2J_3^l+4J_4^l)\cos(2\pi q) \\
& +8J_3^t\cos(3\pi q)+2J_4^t\cos(4\pi q)\ , \\
J^{xy}(\mathbf{q}) = {} & \mp 2(J_1^a+2J_3^{a\,1}+J_4^a)\mp 8J_3^{a\,2}\cos(\pi q) \\
& \pm 2(J_1^a+2J_3^{a\,1})\cos(2\pi q)\pm 8J_3^{a\,2}\cos(3\pi q) \\
& \pm 2J_4^a\cos(4\pi q)\ ,
\end{aligned}
$$

for $\mathbf{q}=(2\pi/a)(q,q,q)$,

$$
\begin{aligned}
J^{zz}(\mathbf{q}) = {} & 2(2J_1^l+J_1^t+J_3^l+2J_3^t+2J_4^l+J_4^t) \\
& +2(2J_1^l+J_1^t+J_2^l+2J_2^t+2J_3^l+4J_3^t)\cos(2\pi q) \\
& +2(J_3^l+2J_3^t+2J_4^l+J_4^t)\cos(4\pi q)\ , \\
J^{xy}(\mathbf{q}) = {} & -2(J_1^a-J_3^{a\,1}+2J_3^{a\,2}+J_4^a) \\
& -2(J_1^a-2J_3^{a\,1})\cos(2\pi q) \\
& +2(J_3^{a\,1}+2J_3^{a\,2}+J_4^a)\cos(4\pi q)\ .
\end{aligned}
$$

For the different elements of the Fourier transformed interaction tensor the following symmetry relations hold:

$$
\begin{aligned}
& J^{xx}(q_1,q_2,q_3)=J^{yy}(q_2,q_3,q_1)=J^{zz}(q_3,q_1,q_2)\ , \\
& J^{xx}(q,0,0)\neq J^{xx}(0,q,0)=J^{xx}(0,0,q)\ , \\
& J^{yy}(0,q,0)\neq J^{yy}(0,0,q)=J^{yy}(q,0,0)\ , \\
& J^{zz}(0,0,q)\neq J^{zz}(q,0,0)=J^{zz}(0,q,0)\ , \\
& J^{xx}(q,0,0)=J^{yy}(0,q,0)=J^{zz}(0,0,q)\ .
\end{aligned}
$$

[1]J. Rossat-Mignod, P. Burlet, S. Quezel, and O. Vogt, Physica **102B**, 237 (1980).
[2]J. Rossat-Mignod, P. Burlet, J. Villain, H. Bartholin, W. Tscheng-Si, and D. Florence, Phys. Rev. B **16**, 440 (1977).
[3]P. Fischer, B. Lebech, G. Meier, B. D. Rainford, and O. Vogt, J. Phys. C **11**, 345 (1978).
[4]F. Levy, Phys. Condens. Matter **10**, 85 (1969).
[5]F. Hulliger, M. Landolt, H. R. Ott, and R. Schmelzer, J. Low Temp. Phys. **20**, 269 (1975).
[6]B. Coqblin and J. R. Schrieffer, Phys. Rev. **185**, 847 (1969).
[7]B. R. Cooper, J. Magn. Magn. Mater. **29**, 230 (1982).
[8]H. Takahashi and T. Kasuya, J. Phys. C **18**, 2695 (1985).
[9]G. H. Lander, S. K. Sinha, D. M. Sparlin, and O. Vogt, Phys. Rev. Lett. **40**, 523 (1978).
[10]S. K. Sinha, G. H. Lander, S. M. Shapiro, and O. Vogt, Phys. Rev. Lett. **45**, 1028 (1980); Phys. Rev. B **23**, 4556 (1981).
[11]T. M. Holden, W. J. L. Buyers, E. C. Svensson, and G. H. Lander, Phys. Rev. B **26**, 6227 (1982).
[12]B. Hälg, A. Furrer, W. Hälg, and O. Vogt, J. Appl. Phys. **53**, 1927 (1982).
[13]B. Hälg, A. Furrer, W. Hälg, and O. Vogt, J. Magn. Magn. Mater. **29**, 151 (1982).
[14]B. Hälg and A. Furrer, J. Appl. Phys. **55**, 1860 (1984).
[15]N. Kioussis and B. R. Cooper, J. Magn. Magn. Mater. **54-57**, 701 (1986); Phys. Rev. B **34**, 3261 (1986).
[16]B. Hälg, A. Furrer, W. Hälg, and O. Vogt, J. Phys. C **14**, L961 (1981).
[17]B. Hälg, A. Furrer, and O. Vogt, Phys. Rev. Lett. **54**, 1388 (1985).
[18]A. Furrer, W. Hälg, H. Heer, and O. Vogt, J. Phys. (Paris) Colloq. **40**, C5-122 (1979).
[19]J. Rossat-Mignod, J. M. Effantin, C. Vettier, and O. Vogt, Physica **130B**, 555 (1985).
[20]G. H. Lander, W. G. Stirling, and O. Vogt, Phys. Rev. Lett. **42**, 260 (1979); Phys. Rev. B **21**, 436 (1980).
[21]T. M. Holden, W. J. L. Buyers, E. C. Svensson, and G. H. Lander, Phys. Rev. B **30**, 114 (1984).
[22]M. Loewenhaupt, G. H. Lander, A. P. Murani, and A. Murasik, J. Phys. C **15**, 6199 (1982).
[23]J. Jensen and P. Bak, Phys. Rev. B **23**, 6180 (1981).
[24]B. R. Cooper, P. Thayamballi, and D. Yang, J. Appl. Phys. **55**, 1866 (1984); Phys. Rev. B **29**, 4049 (1984).
[25]See, e.g., P. Fulde, *Handbook on the Physics and Chemistry of Rare Earths*, edited by K. A. Gschneidner Jr. and L. Eyring (North-Holland, Amsterdam, 1979).
[26]A. Loidl, K. Knorr, J. K. Kjems, and B. Lüthi, Z. Phys. B **35**, 253 (1979).
[27]See, e.g., N. Hessel Andersen, J. Jensen, H. Smith, O. Splittorff, and O. Vogt, Phys. Rev. B **21**, 189 (1980).
[28]P. Burlet, S. Quezel, J. Rossat-Mignod, and O. Vogt, Proceedings of the Symposium on Neutron Scattering, Berlin, 1984 (unpublished).
[29]B. Hälg, A. Furrer, J. K. Kjems, and O. Vogt, Phys. Rev. Lett. **50**, 1085 (1983).
[30]H. Takahashi and T. Kasuya, J. Phys. C **18**, 2755 (1985).
[31]W. Selke and M. E. Fischer, Phys. Rev. B **20**, 257 (1979); M. E. Fischer, J. Appl. Phys. **52**, 2014 (1981); J. v. Boehm and P. Bak, Phys. Rev. Lett. **42**, 122 (1979).
[32]K. W. H. Stevens, Proc. Phys. Soc. London, Sect. A **65**, 209 (1952).
[33]M. J. Sablik and Y. L. Wang, Phys. Rev. B **19**, 2729 (1979); P. Morin, D. Schmitt, and C. Vettier, and J. Rossat-Mignod, J. Phys. F **10**, 575 (1980).
[34]W. Marshall and S. W. Lovesay, *Theory of Thermal Neutron Scattering* (Oxford University Press, London, 1971).
[35]K. Mattenberger, L. Scherrer, and O. Vogt, J. Cryst. Growth **67**, 467 (1984).
[36]H. Heer, A. Furrer, W. Hälg, and O. Vogt, J. Phys. C **12**, 5207 (1979).
[37]G. Meier, P. Fischer, W. Hälg, B. Lebech, B. D. Rainford, and O. Vogt, J. Phys. C **11**, 1173 (1978).
[38]B. Hälg, A. Furrer, and O. Vogt, J. Magn. Magn. Mater. **54-57**, 705 (1986).
[39]K. R. Lea, M. J. M. Leask, and W. P. Wolf, J. Phys. Chem. Solids **23**, 1381 (1962).
[40]B. Reihl, N. Mårtensson, and O. Vogt, J. Appl. Phys. **53**, 2008 (1982).